Errors in Sounding of the Atmosphere using Broadband Emission Radiometry (SABER) kinetic temperature caused by non-local-thermodynamic-equilibrium model parameters

M. García-Comas,[1] M. López-Puertas,[1] B. T. Marshall,[2] P. P. Wintersteiner,[3] B. Funke,[1] D. Bermejo-Pantaleón,[1] C. J. Mertens,[4] E. E. Remsberg,[4] L. L. Gordley,[2] M. G. Mlynczak,[4] and J. M. Russell III[5]

[1] The vast set of near-global and continuous atmospheric measurements made by the Sounding of the Atmosphere using Broadband Emission Radiometry (SABER) instrument since 2002, including daytime and nighttime kinetic temperature (T_k) from 20 to 105 km, is available to the scientific community. The temperature is retrieved from SABER measurements of the atmospheric 15 μm CO_2 limb emission. This emission separates from local thermodynamic equilibrium (LTE) conditions in the rarefied mesosphere and thermosphere, making it necessary to consider the CO_2 vibrational state non-LTE populations in the retrieval algorithm above 70 km. Those populations depend on kinetic parameters describing the rate at which energy exchange between atmospheric molecules take place, but some of these collisional rates are not well known. We consider current uncertainties in the rates of quenching of $CO_2(v_2)$ by N_2, O_2 and O, and the $CO_2(v_2)$ vibrational-vibrational exchange to estimate their impact on SABER T_k for different atmospheric conditions. The T_k is more sensitive to the uncertainty in the latter two, and their effects depend on altitude. The T_k combined systematic error due to non-LTE kinetic parameters does not exceed ±1.5 K below 95 km and ±4−5 K at 100 km for most latitudes and seasons (except for polar summer) if the T_k profile does not have pronounced vertical structure. The error is ±3 K at 80 km, ±6 K at 84 km and ±18 K at 100 km under the less favorable polar summer conditions. For strong temperature inversion layers, the errors reach ±3 K at 82 km and ±8 K at 90 km. This particularly affects tide amplitude estimates, with errors of up to ±3 K.

1. Introduction

[2] The Sounding of the Atmosphere using Broadband Emission Radiometry (SABER) is a broadband radiometer which measures limb radiance emitted from the terrestrial atmosphere in 10 selected spectral bands ranging from 1.27 to 15 μm. SABER, launched aboard the Thermosphere-Ionosphere-Mesosphere Energetics and Dynamics (TIMED) satellite on 7 December 2001, orbits the earth in a 74°

inclined plane. It scans the limb from the surface up to ∼350 km and then back down to the surface in a 110 second sequence with a 2 km field of view and with a very high signal to noise ratio (S/N = 1 at ∼130 km for the 15 μm channels). SABER daily provides about 1500 atmospheric radiance profiles per channel both during day and night covering from 82°N to 53°S (alternating with 53°N to 82°S every 2 months). A more detailed description of SABER performance is given by *Russell et al.* [1999].

[3] One of the main goals of the SABER experiment is to retrieve kinetic temperature (T_k) from 20 to 105 km with a high accuracy. The temperature is needed not only to study the atmospheric dynamics, chemistry and energetics but also to retrieve almost all SABER products. In order to derive T_k, two channels are devoted to register CO_2 infrared emission at 15 μm. These are the narrow and the wide band 15 μm channels (channels 1 and 3), with band passes from

---

[1] Instituto de Astrofísica de Andalucía, CSIC, Granada, Spain.
[2] G & A Technical Software, Newport News, Virginia, USA.
[3] ARCON Corporation, Waltham, Massachusetts, USA.
[4] NASA Langley Research Center, Hampton, Virginia, USA.
[5] Center for Atmospheric Sciences, Hampton University, Hampton, Virginia, USA.

635 to 710 cm^{-1} and 570 to 780 cm^{-1}, respectively. They measure over the spectral region of the CO_2 vibration bending mode energy ($v_2 \simeq 667$ cm^{-1}) with noise equivalent radiances (NER) of 2.45×10^{-4} W sr^{-1}m^{-2} and 3.3×10^{-4} W sr^{-1} m^{-2}, respectively.

[4] In a first step, the pressure and the kinetic temperature are retrieved using the two-channel technique suggested by *Gille and House* [1971] assuming LTE (local thermodynamic equilibrium). However, since the assumption of LTE breaks down in the mesosphere [see, e.g., *López-Puertas and Taylor*, 2001], the T_k is derived in a second step with the algorithm described by *Mertens et al.* [2001], which accounts for nonlocal thermodynamic equilibrium (non-LTE) effects. Thus, it is important to understand the mechanisms that populate the CO_2 vibrational levels emitting at 15 μm. That applies, in particular, to the rates at which energy exchanges between atmospheric molecules take place. Some of these rate coefficients are still not determined with high accuracy and their current uncertainty is the main source of error in the calculation of the level populations. That induces nonnegligible errors in the retrieved parameters. The magnitude of these errors depends on the atmospheric conditions, being larger when the non-LTE effects are more important, i.e., under polar summer conditions or for large-amplitude temperature inversion layers.

[5] *Remsberg et al.* [2008] validate SABER version 1.07 (v1.07 hereafter) temperature from 20 to 100 km and assess the errors related to the retrieval scheme and to the noise and the pointing jitter. They review in detail the errors up to the lower mesosphere due to the approximations assumed in the forward radiance calculations, uncertainties in the channel 3 radiance calibration, selection of the region of pressure registration, and uncertainties in the ozone contribution correction for the channel 3 radiance. The overall (root-sum-squared) estimated random and systematic temperature errors are respectively 0.3 and 1.4 K at 100 mb, 0.3 and 0.7 K at 10 mb, 0.6 and 1.9 K at 1 mb, and 0.7 and 1.5 K at 0.1 mb [see *Remsberg et al.*, 2008, Table 1]. They also provide an estimate of the errors due to the assumed CO_2 profile in the upper mesosphere and lower thermosphere (1.3 K at 80 km, 3.6 K at 90 km, and 1.4 K at 100 km), and the noise error for a single scan (1.8 and 2.7 K at 80 km, 3.6 K and 8.9 K at 90 km, and 6.7 and 8.9 K at 100 km for midlatitude and polar conditions respectively).

[6] The work presented here complements the *Remsberg et al.* [2008] paper in that it assesses the errors induced by the current uncertainties in the non-LTE model collisional rates on the temperature in the Mesosphere and Lower Thermosphere (MLT), which are added to the systematic errors [see *Remsberg et al.*, 2008, Table 2]. We estimate those errors using SABER measurements taken during typical and extreme conditions, and different seasons. In section 2 we describe the main features of the atmospheric emission at 15 μm in the MLT region, summarize the SABER non-LTE T_k retrieval code and refer to the SABER data used for this analysis. In section 3 we review the collisional rate coefficients used in the non-LTE model whose uncertainties most affect the T_k retrieval and report the systematic errors on the retrieved T_k caused by the current uncertainties in those collisional parameters. In

section 4, we summarize our results and draw our conclusions.

2. SABER Non-LTE Kinetic Temperature

[7] Mesospheric and lower thermospheric kinetic temperature is retrieved from SABER atmospheric 15 μm radiance measurements considering non-LTE effects. *Mertens et al.* [2001, 2002] describe in detail the non-LTE retrieval algorithm used operationally to derive that kinetic temperature (non-LTE T_k hereafter) above 40 km. This code is composed of two main components: (1) the forward model and (2) the inversion model.

[8] The forward calculations at 15 μm are performed with the BANDPAK algorithm [*Marshall et al.*, 1994] after the populations (i.e., the vibrational temperatures) of the CO_2 vibrational levels are supplied by a non-LTE model. This model includes all known excitation and relaxation mechanisms of the states, i.e., collisional processes (thermal collisions, vibrational energy transfer, electronic to vibrational energy transfer) and radiative processes (energy exchange between atmospheric layers, absorption of solar radiation, spontaneous and induced emission), as described by *López-Puertas and Taylor* [2001]. The vibrational temperatures (T_v hereafter) calculated with the SABER non-LTE model were validated against those from the ARC [*Wintersteiner et al.*, 1992], the IAA [*López-Puertas et al.*, 1986, 1998] and the ALI [*Kutepov et al.*, 2006] non-LTE models from 40 to 160 km. SABER operational non-LTE and IAA codes solve the radiative transfer problem using the Curtis matrix method, whereas the ARC and the ALI (Accelerated Lambda Iteration) codes use an iteration technique. All models included the same collisional rate constants in the intercomparison. The differences between the models are smaller than 1 K for all levels included at all altitudes considered.

[9] The inversion code consists of two nested relaxation loops. In the inner loop, kinetic temperature is retrieved with an onion peeling procedure using a Levenberg-Marquardt approach. This module is iteratively run until the convergence criterion is met, i.e., until the difference in the simulated radiance at every tangent height between two successive iterations is less than the noise error. In the outer loop the pressure is hydrostatically rebuilt and the vibrational temperatures are again calculated. The outer loop convergence criterion requires the root-sum-square (RSS) of the difference of two successive T_k profiles over all retrieved altitudes be less than the RSS of the expected solution errors (noise-induced) over all retrieved altitudes.

[10] In order to understand the response of the non-LTE retrieval to changes in the collisional parameters, we briefly describe here the behavior of the CO_2 vibrational level populations and their contributions to SABER 15 μm channels. We will use hereafter the Herzberg notation to refer to the vibrational levels, i.e., (v_1, v_2^l, v_3), where v_1, v_2, v_3 designate the level excited in the symmetric stretching, the bending and the asymmetric stretching modes, respectively, and l is the vibrational angular momentum quantum number. We will also denote the CO_2 isotopes with the last digit of the atomic weight of each atom, for example, 626 isotope for $^{12}C^{16}O_2$.

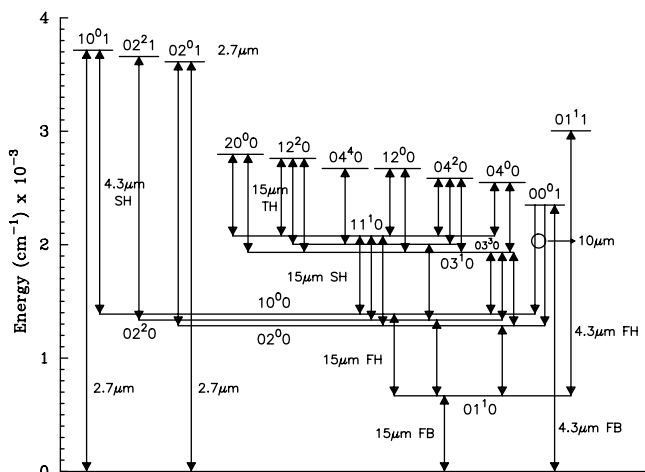**Figure 1.** Energy of the main CO_2 vibrational states. The arrows show the main CO_2 bands emitting at 15, 10, and 4.3 μm (FB, fundamental band; FH, first hot band; SH, second hot bands; and TH, third hot band).

[11] The vibrational levels and bands which, directly or indirectly, affect the CO_2 emission at 15 μm measured by SABER are shown in Figure 1. The fractional contributions at non-LTE altitudes to the total SABER 15 μm channel 1 radiance of the CO_2 vibrational bands (see bands included in the model of *Mertens et al.* [2002]) for a standard case are shown in Figure 2. We have estimated those from simulated profiles using the US Standard 76 atmosphere [*Fleming et al.*, 1990]. Although the fractional contributions depend on the atmospheric conditions, these results are representative of the general behavior. The 626-CO_2 v_2 fundamental band (01^10-00^00) is the main contributor to the 15 μm channel total radiance at all altitudes although the first hot band (10^00-01^10, 02^20-01^10 and 02^00-01^10) and the minor isotope (636, 628, 627) fundamental band contributions reach 30% at 85 and 75 km, respectively. The contribution from the remaining bands (rest of CO_2 hot bands and ozone v_2 fundamental band) is less than 5% above 70 km.

[12] SABER temperatures from version 1.07 were retrieved assuming: (1) CO_2 volume mixing ratio (vmr hereafter) from monthly and diurnal averages from the Whole Atmosphere Community Climate Model (WACCM) [*García et al.*, 2007 and references therein], (2) N_2, O_2, nighttime O and daytime O (above 95 km) vmr from NRL-MSISE-00 [*Picone et al.*, 2002]; (3) SABER daytime O (below 95 km) as inferred from the O_3 retrieval of SABER 1.27 μm channel [*Mlynczak et al.*, 1993, 2007]; (4) the nominal values of the collisional rate coefficients (see *López-Puertas and Taylor* [2001, Table 6.2], *Kutepov et al.* [2006], and discussion below). Also, the non-LTE T_k is merged with the LTE T_k around ~65 km.

[13] Figure 3 shows zonal mean (latitude cross section) maps of SABER v1.07 kinetic temperature for equinox (18 March 2004) and solstice (15 July 2004). We selected these two days because yaw maneuvers were performed then, hence, SABER latitudinal coverage is the largest, from 82°S to 82°N. Whereas the kinetic temperature in the MLT during the equinox is almost latitude-independent (except for the stronger tidal signatures at low latitudes and perhaps

a slightly warmer lower mesosphere in the northern most latitudes), the northern summer solstice distribution shows the typical mesopause positive temperature gradient toward the winter polar region during the solstice, together with a lower mesopause in the summer polar region. Since the atomic oxygen is very important in the SABER T_k determination in the upper mesosphere and the lower thermosphere (see section 3.2 for a detailed discussion), we also show the zonal mean daytime and nighttime atomic oxygen mixing ratio used in v1.07 T_k retrieval for the selected days (Figure 4). *Remsberg et al.* [2008] shows examples of the CO_2 vmr profiles used.

[14] Figure 5 shows v1.07 averaged kinetic temperature profiles together with the corresponding vibrational temperatures for the main CO_2 v_2 levels calculated with the SABER operational non-LTE model for a typical atmospheric scenario (midlatitudes) and two extreme cases (polar summer and polar winter). We calculated those zonal means using all SABER temperature profiles measured within 10° latitude bins during 15 January 2003 for the midlatitude conditions and 15 July 2004 for the polar conditions. The average latitude of these zonal mean profiles is 49°S, 79°N and 69°S, respectively.

[15] The behavior of the v_2 level vibrational temperatures is mainly driven by the thermal structure [*López-Puertas and Taylor*, 2001]. In the polar summer, the populations of the 15 μm levels are further away from LTE. In particular, the 626-01^10 level (responsible for the main contribution to SABER 15 μm radiance) is significantly overpopulated with respect to LTE conditions (its vibrational temperature is larger than the T_k) in the polar summer from 75 km to 90 km, whereas it is similarly or less populated (its vibrational temperature is similar or smaller than the T_k) at midlatitudes and in polar winter, where the radiative equilibrium conditions are closer to the thermal balance. That happens because, besides collisions with other molecules (not very frequent in this low-pressure region), absorption
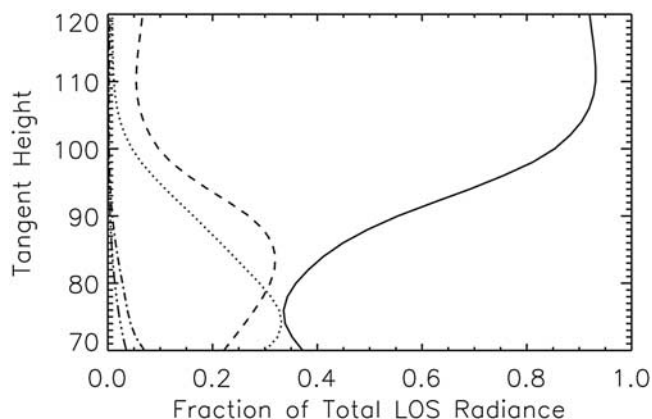

Figure 2. Fractional contribution of CO_2 vibrational bands to SABER Channel 1 (15 μm) simulated radiance for a typical midlatitude profile. Solid line is 626 fundamental band, dashed line is 626 first hot bands, dash-dotted line is 626 second hot bands, dotted line is 636+628+627 fundamental bands, and dash-triple-dotted line is the remainder (see text for more details).
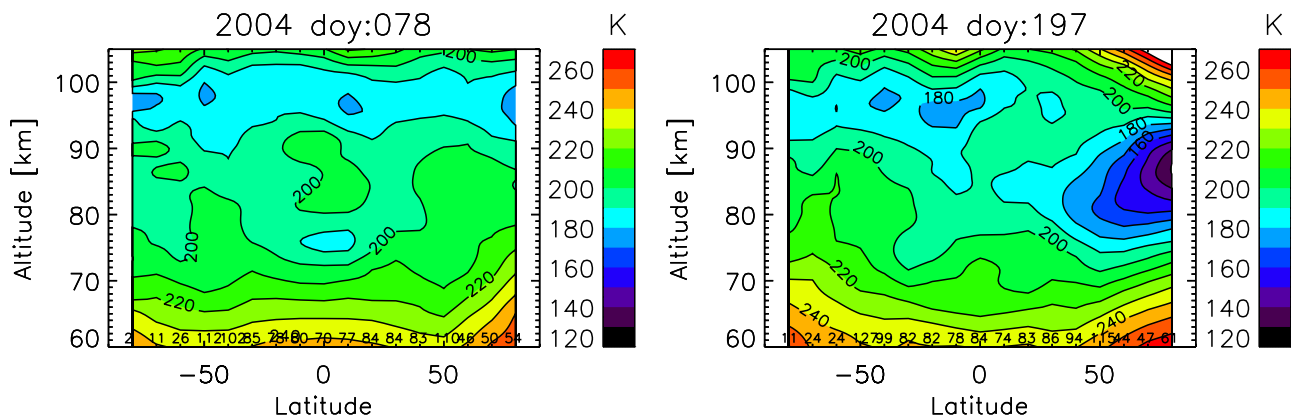
Figure 3. SABER v1.07 kinetic temperatures for (left) equinox (18 March 2004) and (right) solstice (15 July 2004). The contours are every 10 K. Numbers at bottom *x* axis indicate the number of averaged profiles.

of radiation emitted at lower warm atmospheric layers increases the population of the vibrational levels in that altitude range. In polar summer, the warmer stratopause together with the colder mesopause make the vibrational temperatures larger than the kinetic temperature around the mesopause. In midlatitudes and polar winter, the mesopause temperature is not as low and, thus, the absorption of upwelling radiation is not enough for the vibrational temperatures to overcome the local kinetic temperature. Above about 90 km, the 626-01^{1}0 level population is smaller than in LTE under all conditions because collisions are not frequent enough to counteract the emission to space in the 01^{1}0-00^{0}0 band. Besides, the populations of the 626-01^{1}0, the 626-020 (group composed by the 10^{0}0, 02^{2}0, and 02^{2}0 levels) and the 636-01^{1}0 levels, depart from LTE at lower altitudes (70–75 km) in the polar regions. As we show in section 3, the larger the deviation from LTE conditions, the larger the impact of perturbations of the collisional

rates and, therefore, the larger the error on the retrieved kinetic temperature.

3. Kinetic Parameter Uncertainty Ranges and Errors on SABER T$_k$

[16] The full set of collisional processes used in SABER CO_2 non-LTE model is described by *López-Puertas and Taylor* [2001]. We have considered here the four collisional non-LTE processes that most affect the $CO_2(v_2)$ populations and hence the retrieved T$_k$. They are summarized in Table 1 together with their nominal rate coefficients (as used in version 1.07) and the uncertainties assumed in this work. The selection of these values is based on considerations made by *Wintersteiner et al.* [1992], *López-Puertas et al.* [1998], *López-Puertas and Taylor* [2001] and *Kutepov et al.* [2006] and are discussed below. There are other non-LTE processes included in the SABER non-LTE model that have
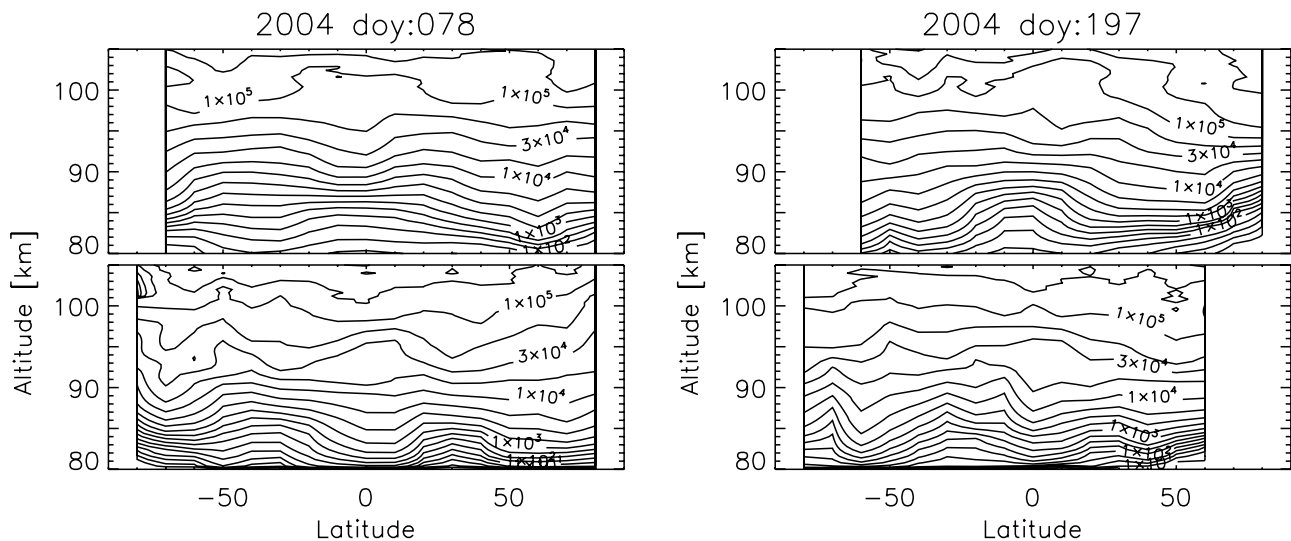

Figure 4. Contour plots of (top) daytime and (bottom) nighttime atomic oxygen mixing ratio (in ppmv) used in SABER v1.07 kinetic temperature retrieval for (left) equinox (18 March 2004) and (right) solstice (15 July 2004). The contours are drawn differing in a factor of 10$^{0.25}$ ppmv.
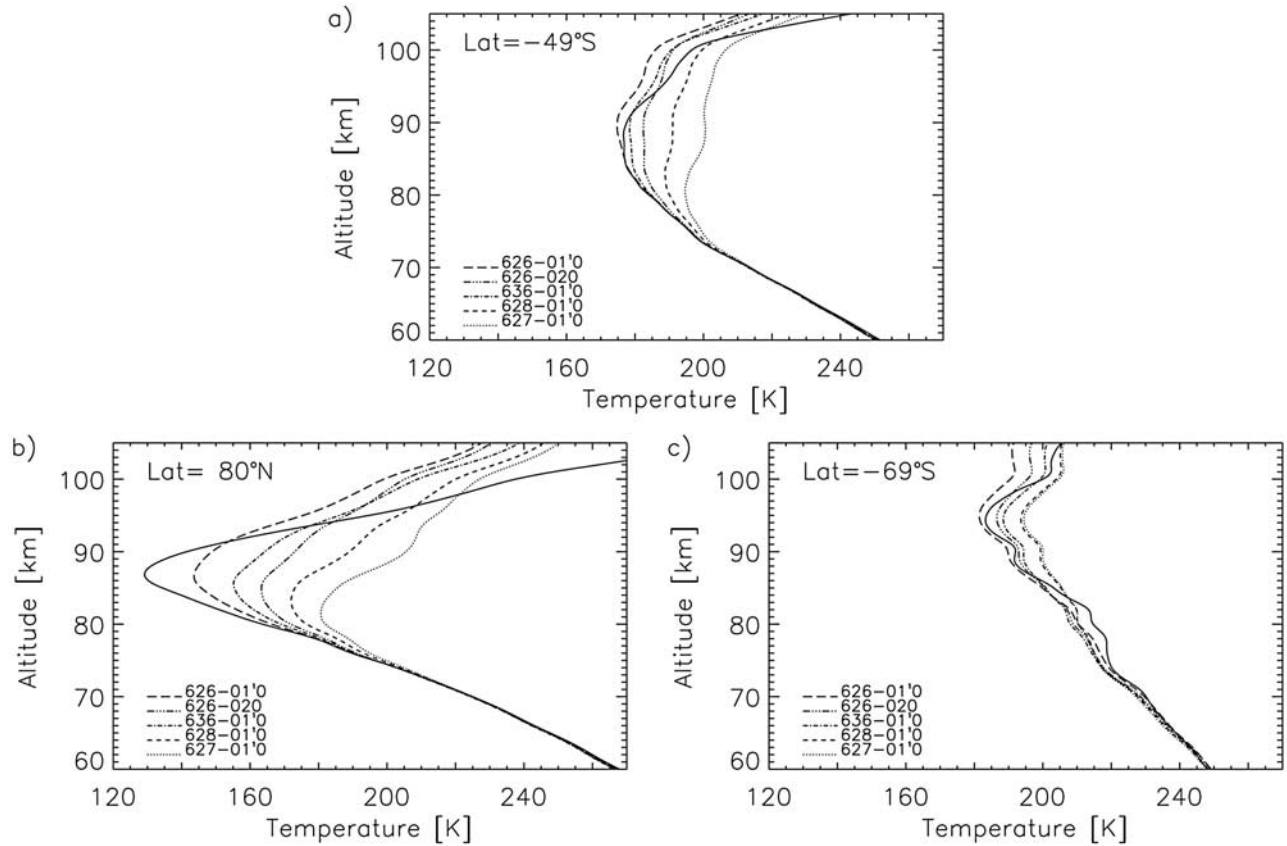
Figure 5. SABER vibrational temperatures of the main CO_2 v_2 vibrational states contributing to the 15-μm channel typical of (a) midlatitudes, (b) polar summer, and (c) polar winter. The profiles are zonal means for $10°$ latitude boxes at the average latitude shown. The solid line is the kinetic temperature.

a nonnegligible uncertainty but they do not yield significant errors in the retrieved temperatures.

[17] To estimate the T_k errors caused by those uncertainties, we have perturbed the nominal rate constants used in the model and performed T_k retrievals. Comparisons with the kinetic temperature retrieved using the nominal values in v1.07 (nominal T_k hereafter) allow for an estimate of these systematic errors. The response of the retrieval to perturbations of the collisional rates is to compensate for the change induced in the vibrational temperatures by modifying the kinetic temperature to restore the T_vs close to their nominal values so that SABER 15 μm radiance is again matched. As

shown below, the T_k response to the considered increase or decrease of the rate coefficients is not symmetrical about the nominal value because the behavior of the non-LTE populations and the radiative transfer are nonlinear. Besides, the magnitude of these T_k errors depends on the thermal structure, more strongly affecting the profiles retrieved for those conditions in which the vibrational levels are farther from LTE, for example, under polar summer conditions or when strong inversion layers are present.

[18] We have fulfilled those calculations for the two typical days during 2004 in equinox and solstice (18 March and 15 July) whose nominal zonal mean T_k is shown in

Table 1. Collisional Processes for the CO_2 Vibrational Levels Relevant to This Work, Corresponding Nominal Collisional Rates, and Associated Uncertainty Factors

Process Number	Process[a]	Collisional Rate[b]	Uncertainty Factor
1	$CO_2^i(v_2) + N_2 \rightleftharpoons CO_2^i(v_2 - 1) + N_2$	$k_{CO2\text{-}air1} = A_{v_2}[7 \times 10^{-17} \sqrt{T} +$ $+6.7 \times 10^{-10}\exp(-83.8/T^{1/3})]$	$0.75 - 1.25$
2	$CO_2^i(v_2) + O_2 \rightleftharpoons CO_2^i(v_2 - 1) + O_2$	$k_{CO2\text{-}air2} = A_{v_2}[7 \times 10^{-17} \sqrt{T} +$ $+1.0 \times 10^{-9}\exp(-83.8/T^{1/3})]$	$0.75 - 1.25$
3	$CO_2^i(v_2) + O(^3P) \rightleftharpoons CO_2^i(v_2 - 1) + O(^3P)$	$k_{CO2\text{-}O} = 3.5 \times 10^{-13} \sqrt{T} +$ $+2.3 \times 10^{-9}\exp(-76.75/T^{1/3})$	$0.5 - 1.5$
4	$CO_2^i(v_2) + CO_2^j(v'_2) \rightleftharpoons CO_2^i(v_2 - 1) + CO_2^j(v'_2 + 1)$	$k_{vv} = 1.2 \times 10^{-11}$ if $i = j$ & $v'_2 = 0$ $= 2.4 \times 10^{-11}$ if $v_2 = v'_2 + 1 = 1$	see text

[a]Here i and j denote different CO_2 isotopes.
[b]Rates in the forward sense of the process are given in cm^3s^{-1}. $A_{v_2=1} = 1$ and $A_{v_2 \neq 1} = 3\frac{g_{v_2}}{g_2}$, where g_{v_2} is the degeneracy of level v_2.
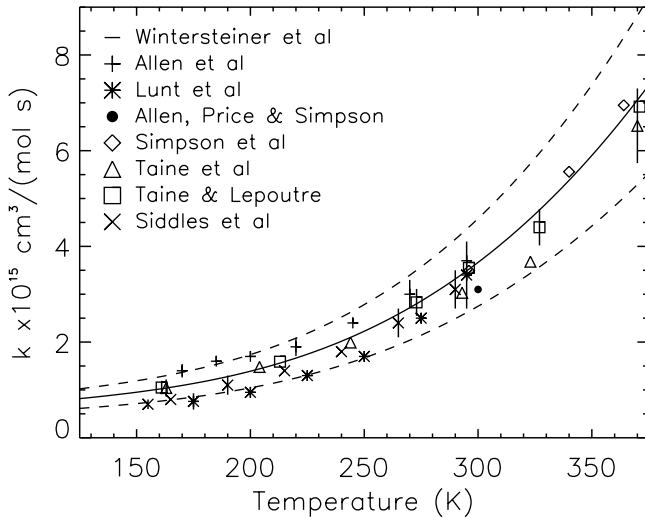
Figure 6. Reported values for the relaxation rate of $CO_2(v_2)$ by molecular nitrogen. The solid line corresponds to the value adopted in v1.07, and the dashed lines indicate the uncertainty range assumed in this work. Solid line also denotes data from *Wintersteiner et al.* [1992]. Vertical bars denote measurement errors. Other data sources are denoted as follows: plus, *Allen et al.* [1980]; asterisk, *Lunt et al.* [1985]; dot, *Allen et al.* [1977]; diamond, *Simpson et al.* [1977]; triangle, *Taine et al.* [1978]; square, *Taine and Lepoutre* [1979]; and cross, *Siddles et al.* [1994].

Figure 3. We have also analyzed the impact of the collisional rate uncertainties for some extreme cases in which we expect to find larger errors, for example, those with strong inversion layers in the MLT or a high stratopause. We have studied the effect of the collisional rates of processes 3 and 4 independently whereas we have considered the combined effect of processes 1 and 2, since both produce a similar effect.

[19] In the next sections, we justify the selection of the uncertainty ranges for each individual process shown in Table 1 and analyze in detail their effect on the SABER T_k. Although not a non-LTE parameter, the uncertainty in the atomic oxygen also induces T_k errors through the non-LTE population calculations. Those errors are also briefly discussed below. The errors due to uncertainties in the CO_2 vmr, however, affect the forward radiance through the CO_2 density but not through the non-LTE populations since the effect of CO_2 abundance on the vibrational temperatures is small [*López-Puertas and Taylor*, 2001]. Those errors are assessed by *Remsberg et al.* [2008].

3.1. Processes 1 and 2: $CO_2^i(v_2) + M(N_2, O_2) \rightleftharpoons CO_2^i(v_2 - 1) + M(N_2, O_2)$

[20] Thermal collisions of carbon dioxide with molecular nitrogen and molecular oxygen (processes 1 and 2) keep the v_2 states in LTE up to the middle mesosphere. The values for the rate coefficient reported in the literature for quenching of $CO_2(v_2)$ by N_2 are summarized in Figure 6. *Taine et al.* [1978] and *Allen et al.* [1980] measured the rate of collisions with molecular nitrogen at atmospheric temperatures but only for low-energy vibrational levels. There are also laboratory measurements of this coefficient reported by

Simpson et al. [1977], *Allen et al.* [1977], *Taine and Lepoutre* [1979], *Lunt et al.* [1985] and *Siddles et al.* [1994]. All measurements gave similar values within their experimental errors. *Simpson et al.* [1977], *Taine et al.* [1978] and *Siddles et al.* [1994] also provided the rate of $CO_2(v_2)$ relaxation in collisions with molecular oxygen (see Figure 7). The nominal values for both coefficients ($k_{CO2\text{-}air}$) used here are the parameterizations of *Wintersteiner et al.* [1992] obtained by fitting the aforementioned experimental data. On the basis of those experiments, we have assumed a $[-25\%, 25\%]$ uncertainty in the rates of both processes. Uncertainties in the temperature dependence are also included in that range.

[21] Figure 8 shows zonal mean maps of the errors in the retrieved kinetic temperature due to this process for the two typical days during equinox (Figure 8, left) and solstice (Figure 8, right) studied here. As with the other collisional rates, the operational T_k retrieval responds as expected to the perturbations of the rate constants: the maps for equinox and solstice at the top of Figure 8 are almost completely anticorrelated with the corresponding maps at the bottom.

[22] The v_2 fundamental band upper vibrational levels (01^10) of all the CO_2 isotopes and the first hot band upper levels, main emitters at 15 μm in the middle and upper mesosphere, remain close to LTE up to $\sim85-90$ km under typical midlatitude conditions (see Figure 5a). The uncertainty range of the rate of $CO_2(v_2)$ quenching by N_2 and O_2 is not large enough to change the altitude of the LTE breakdown significantly and, therefore, the effect on the SABER retrieved T_k is small. That is also the case for polar winter and at all latitudes during the equinox (see Figure 8), where the errors are always smaller than ±0.5 K.

[23] In polar summer, the 01^10 levels start to depart from LTE at lower altitudes, in particular those of the minor isotopes. Hence, the retrieved kinetic temperature is more affected than in midlatitudes. The uncertainty of these rates produces maximum errors of ±2 K in polar summer conditions at 85 km. It is worth pointing out that, even though the errors are small at most latitudes, the effect of increasing or decreasing the collisional rate is the opposite for the
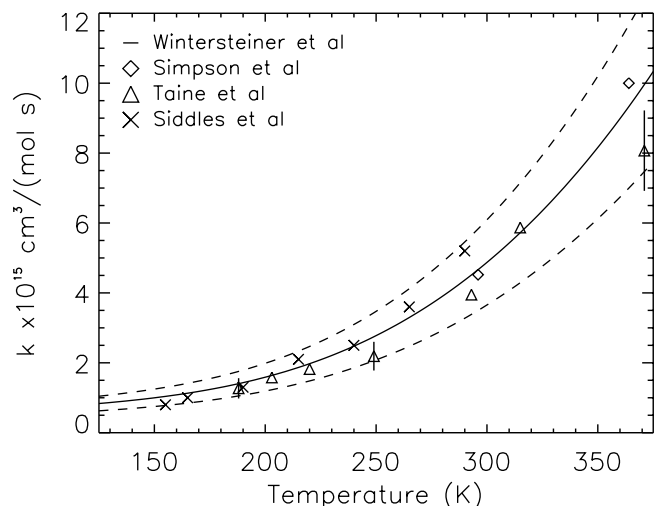

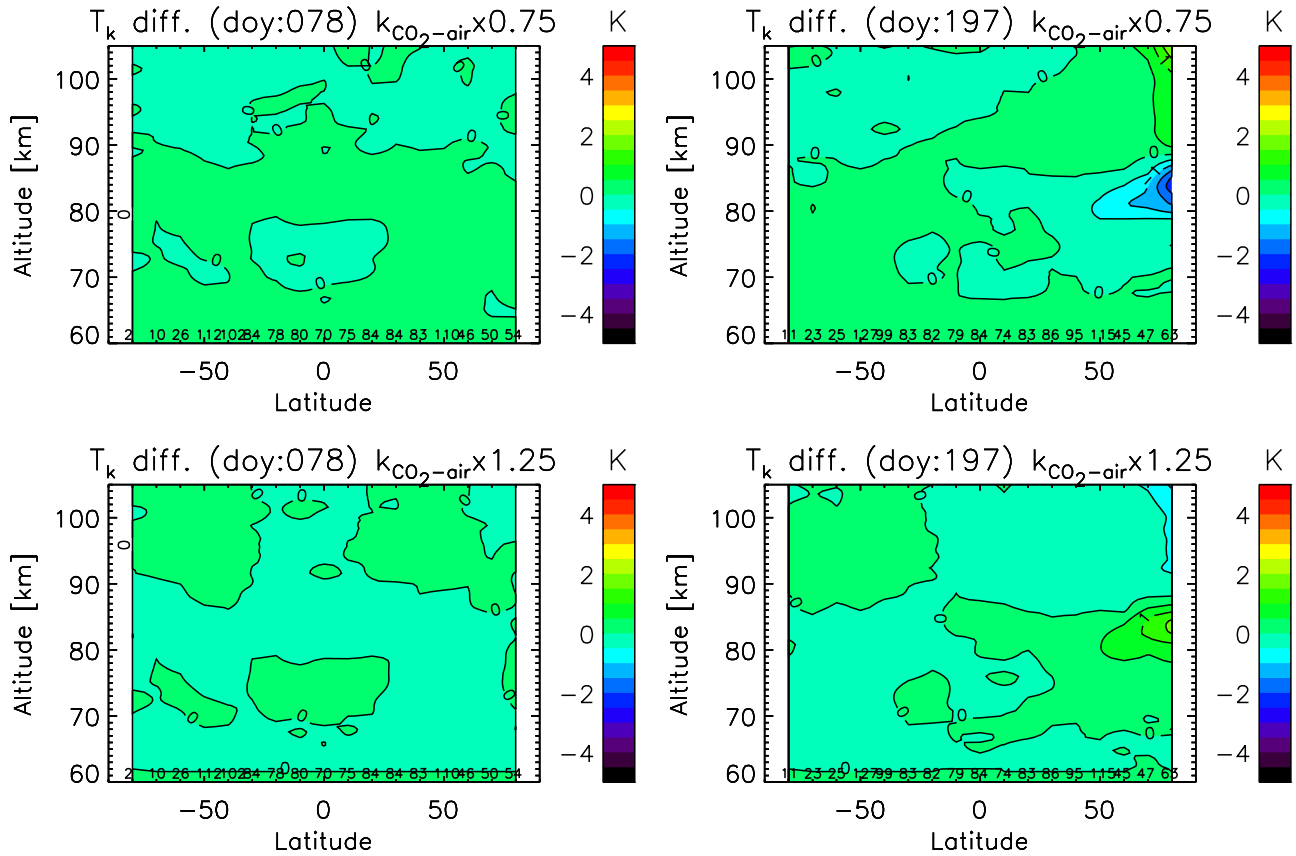**Figure 7.** As in Figure 6 but for the relaxation rate of $CO_2(v_2)$ by molecular oxygen.

Figure 8. Errors in SABER T_k caused by the uncertainty in the $CO_2(\upsilon_2)$ quenching rate by N_2 and O_2 for (left) 18 March (equinox) and (right) 15 July (solstice) 2004 for (top) $k_{CO2\text{-}air} \times 0.75$ and (bottom) $k_{CO2\text{-}air} \times 1.25$. These errors correspond to the temperature maps of Figure 3. Contours are plotted every 0.5 K.

summer and the winter scenarios below 90 km. This is because the 626-01^{1}0 state is more populated than in LTE in the polar summer mesosphere while less populated in polar winter (see Figures 5b and 5c).

3.2. Process 3: $CO_2^i(\upsilon_2) + O(^3P) \rightleftharpoons CO_2^i(\upsilon_2 - 1) + O(^3P)$

[24] Process 3 plays an important role in the radiative cooling of the terrestrial thermosphere since it exerts a major influence on the $CO_2(\upsilon_2)$ state populations in this region. Until the beginning of the past decade and owing to the lack of direct measurements, there were no reliable data for this collisional coefficient. However, several values of this rate have been reported in the literature since then, some deduced from atmospheric observations (pointing to the largest values) and others measured in the laboratory (suggesting the lowest values) (see Figure 9). Values at 300 K range from $6 \times 10^{-12} cm^3 s^{-1}$ [*Sharma and Wintersteiner*, 1990] (deduced from the SPIRE rocket atmospheric observations) to $1.5 \times 10^{-12} cm^3 s^{-1}$ [*Shved et al.*, 1991; *Pollock et al.*, 1993] (from laboratory measurements).

[25] *Khvorostovskaya et al.* [2002] carried out the first laboratory measurements in the 206–358 K range reporting $1.5 \times 10^{-12} cm^3 s^{-1}$. More recently, *Castle et al.* [2006] have obtained a slightly larger value ($1.8 \times 10^{-12} cm^3 s^{-1}$) from measurements taken at room temperatures. As an exception from other values found in the literature, *Lilenfeld* [1994] measured a very low rate of $0.5 \times 10^{-12} cm^3 s^{-1}$.

López-Puertas et al. [1992] deduced a value at 300 K of $3-6 \times 10^{-12} cm^3 s^{-1}$ from ATMOS measurements and *Grossmann et al.* [2002] corroborated the value of *Sharma and Wintersteiner* [1990] using CRISTA-2 measurements (after comparison with MSIS data), i.e., both closer to the upper limit previously reported. *Gusev et al.* [2006] also claimed that the Sharma and Wintersteiner rate constant used to retrieve kinetic temperature from CRISTA-1 and CRISTA-2 measurements was consistent with the global CRISTA 15 μm measurements above 120 km. The lowest value derived from atmospheric measurements so far reported is that by *Vollman and Grossmann* [1997], who, after the analysis of SISSI data, suggested a rate of $1.5 \times 10^{-12} cm^3 s^{-1}$. However, *Gusev et al.* [2006] pointed out that this low value was most probably due to an unrealistically large CO_2 number density in the lower thermosphere (more than 4 times larger than usual) used in the analysis.

[26] The nominal value used in v1.07 for this rate constant ($k_{CO2\text{-}O}$) is that reported by *Sharma and Wintersteiner* [1990], corroborated by all other atmospheric measurements, including their suggested temperature dependence. Although the laboratory measurements of $k_{CO2\text{-}O}$ are grouped around a lower rate, the atmospheric measurements do not support that value, clearly pointing to a rate of collisions about 4 times larger, i.e., that of Sharma and Wintersteiner. Since v1.07 SABER T_k retrievals use that upper limit rate, we have assumed the uncertainty range
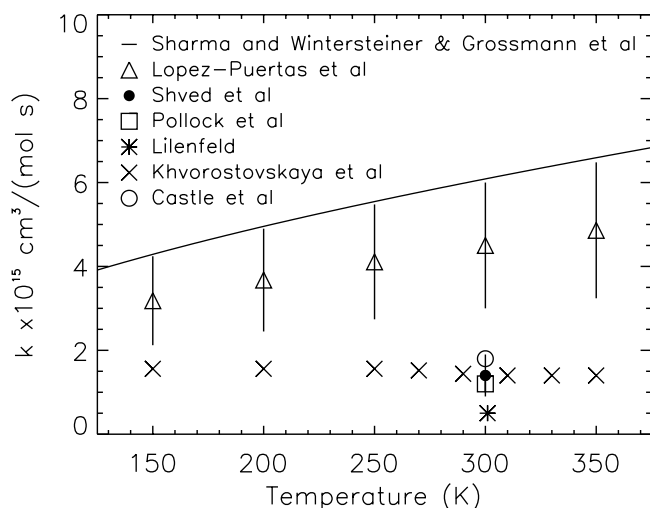
Figure 9. Reported values for the relaxation rate of $CO_2[01^10]$ by atomic oxygen. Besides values adopted in v1.07, solid line also denotes data from *Sharma and Wintersteiner* [1990] and *Grossmann et al.* [2002]. Vertical bars denote measurement errors. Data sources are denoted as follows: solid line, *Sharma and Wintersteiner* [1990] and *Grossmann et al.* [2002]; triangle, *López-Puertas et al.* [2004]; dot, *Shved et al.* [1991]; square, *Pollock et al.* [1993]; asterisk, *Lilenfeld* [1994]; cross, *Khvorostovskaya et al.* [2002]; and circle, *Castle et al.* [2006].

provided by Sharma and Wintersteiner, i.e., [−50%, +50%]. The uncertainty of the temperature dependence of this rate is also included.

[27] The quenching of CO_2 by atomic oxygen is a key process for determining the kinetic temperature from measurements at 15 μm in the upper mesosphere and lower thermosphere, where O is abundant. The latitudinal and seasonal dependence of the errors due to the k_{CO2-O} uncertainty is shown in Figure 10. In order to explain these errors, it is useful to understand first the response of the vibrational temperatures to k_{CO2-O} perturbations.

[28] Lowering the rate of collisions between $CO_2(\nu_2)$ and atomic oxygen leads to ν_2 level populations farther away from LTE. Figure 11a shows the effect on the vibrational temperatures of the main $CO_2(\nu_2)$ vibrational states when dividing the rate by two for a typical midlatitude scenario. The altitude at which the $CO_2(\nu_2 = 1)$ levels of all isotopes depart from LTE barely changes because the effect on their populations is only important a few kilometers above the altitude of LTE breakdown. Since the T_νs of the 626-01^10 and 636-01^10 states are smaller than the T_k, reducing the coupling to the kinetic temperature by lowering the rate k_{CO2-O} further decreases them above $80-85$ km (by 3 K and 1 K, respectively, at 95 km). Although the opposite happens to the 01^10 levels of the 628 isotope (its T_ν increases $2-3$ K at 95 km), the overall effect is to decrease the 15 μm forward limb radiance. This is compensated by an increase in the retrieved T_k to match the SABER radiance; that is, the
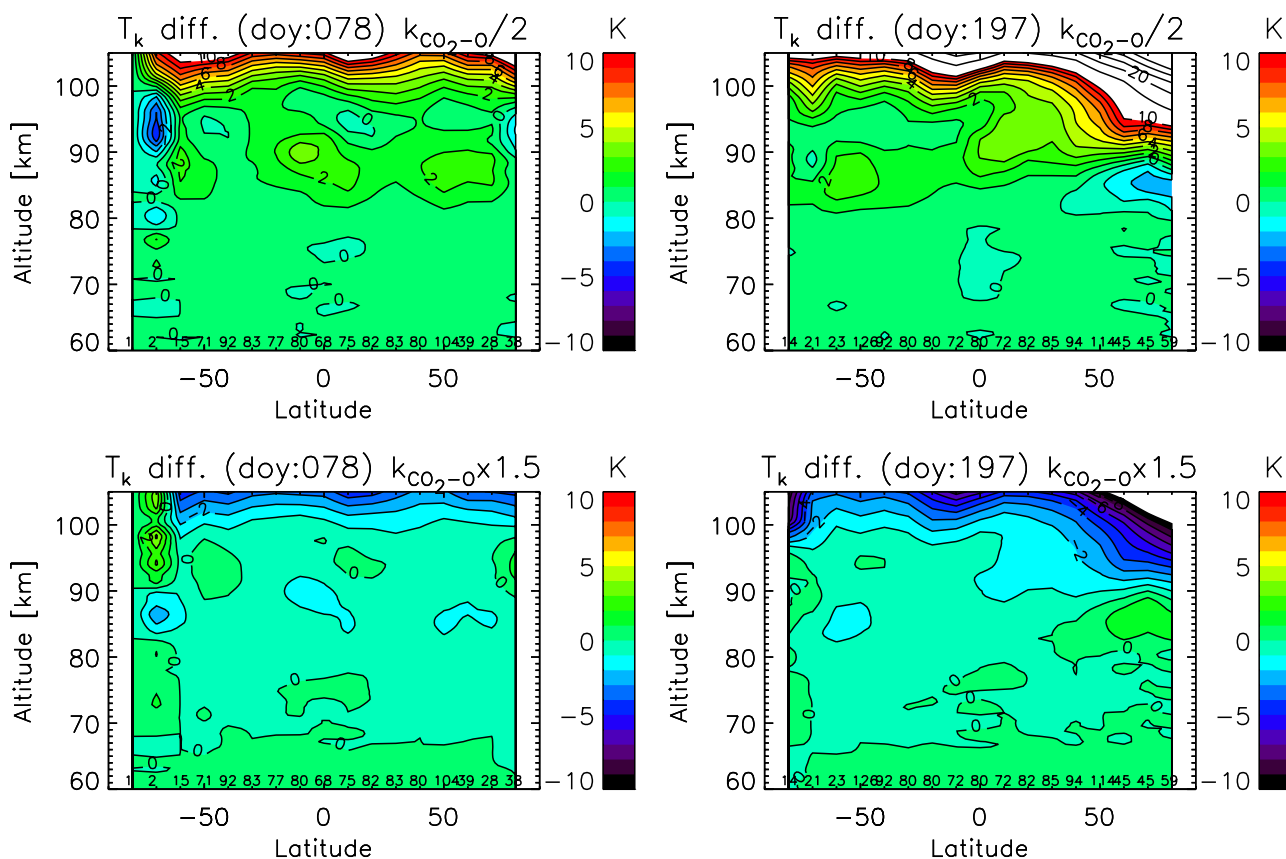

Figure 10. As in Figure 8 but for the uncertainty in $CO_2(\nu_2)$ quenching rate by atomic oxygen for (top) $k_{CO2-O} \times 0.5$ and (bottom) $k_{CO2-O} \times 1.5$. Contours are plotted every 1 K.
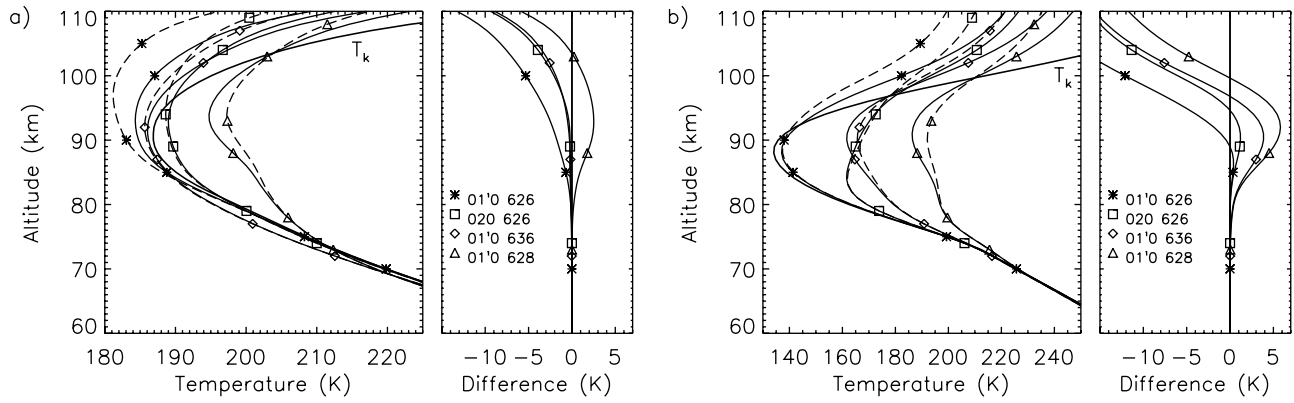
Figure 11. (left) Effect on the $CO_2(v_2)$ vibrational temperatures of reducing the quenching rate of CO_2 with atomic oxygen by a factor of 2 (solid line denotes nominal and dashed line denotes perturbed) for typical (a) midlatitude and (b) polar summer conditions. The kinetic temperature is also shown. (right) Differences correspond to the perturbed minus the nominal vibrational temperature profiles for each level. Lines with symbols correspond to the vibrational levels indicated in the legend.

induced error is positive. The errors in the kinetic temperatures in the positive sense are $1-2$ K from 84 to 96 km, 5 K at 100 km and up to 11 K at 104 km for most latitudes except for polar summer.

[29] In contrast, increasing k_{CO2-O} brings the 01^10 level populations closer to LTE. The T_vs of all levels increase, except for the weaker 628 and 627 isotopic 01^10 levels that decrease between 80 and 100 km. In that case, the resulting T_k decreases at all altitudes with respect to the nominal case. The errors in the negative sense are smaller (in absolute value) than 1 K below 96 km, and from -1 to -2.5 K from 100 to 104 km (see Table 2).

[30] Except for polar summer conditions (discussed below), the response of the retrieved T_k to changes in this rate is similar for all latitudes and seasons (see Figure 10). For polar winter scenarios, the effect appears a few kilometers lower since the 01^10 states depart from LTE at lower altitudes but, as in midlatitudes, increasing k_{CO2-O} leads to a decrease in the retrieved T_k at all altitudes (see also Table 3). Also, as we discuss in more detail later, the errors are larger in the tropics mainly owing to tidally induced variability in

the kinetic temperature vertical structure. That is also the case for the three maxima in the T_k error ($3-4$ K) found for equinox conditions at $85-90$ km around 70°S, 10°S and 50°N (see Figure 10, top left), not typical of this season but caused by inversion layers at those latitudes (see Figure 3).

[31] For polar summer conditions, the v_2 levels are overpopulated with respect to LTE around the mesopause region and less populated at altitudes above around $90-100$ km (see Figure 11b). Therefore, when decreasing the k_{CO2-O} rate by 50%, the vibrational temperatures of all 15 μm CO_2 levels increase in the altitude range of 80 to $\sim$95 km (from 1 K for the 626-01^10 level at 85 km to 6 K for the 01^10 minor isotopic levels at 92 km) but decrease in the region above (up to 12 K at 100 km for 626-01^10). Accordingly, the retrieved kinetic temperature decreases with respect to the nominal T_k in the mesopause region (-2.6 K at 84 km) and increases above (from 6.6 K at 92 km to 40 K at 104 km) (see also Table 4). The opposite happens when increasing the collisional rate by 50%, which yields errors of 1 K at 84 km and from -1.6 K at 92 km to -10 K at 104 km, respectively. The retrieved T_k is almost insensitive to this

Table 2. Uncertainties in Retrieved Kinetic Temperature due to the Specified Uncertainty in the Collisional Rates as in Table 1 for Midlatitude Conditions[a]

z (km)	$k_{CO2-air}$			k_{CO2-O}[b]			k_{vv}			Total		
	-25%	25%	typ	-50%	50%	typ	1.2[c]	2.4[c]	typ	max^-	max^+	typ
104	0.0	0.0	±0.0	11	-3.8	±8.3	0.1	-0.2	±0.1	-3.9	11	±8.3
100	0.0	0.0	±0.0	4.8	-1.7	±3.6	0.1	-0.1	±0.1	-1.8	4.7	±3.6
96	0.0	0.0	±0.0	1.9	-0.6	±1.4	0.1	-0.1	±0.1	-0.6	2.0	±1.4
92	0.0	0.0	±0.0	1.7	-0.5	±1.3	0.1	-0.1	±0.1	-0.5	1.8	±1.3
88	0.0	0.0	±0.0	1.7	-0.5	±1.3	0.0	0.0	±0.0	-0.5	1.8	±1.3
84	0.1	-0.1	±0.1	1.0	-0.5	±0.8	-0.3	0.1	±0.2	-0.8	1.3	±0.8
80	0.1	-0.1	±0.1	0.3	-0.2	±0.3	-0.5	0.1	±0.3	-0.8	0.5	±0.4
76	0.1	0.0	±0.1	0.0	0.0	±0.0	-0.1	0.0	±0.1	-0.3	0.1	±0.1

[a]Temperatures are given in K. The columns labeled typ are the typical errors due to each rate, calculated with the quadratic average of the errors in both senses. Total is the combined error due to the three rate constants in which: max^- (estimated using $k_{CO2-air}^{max}$, k_{CO2-O}^{max}, and k_{vv}^{min} below 88 km and k_{vv}^{max} above) and max^+ (estimated using $k_{CO2-air}^{min}$, k_{CO2-O}^{min}, and k_{vv}^{max} below 88 km and k_{vv}^{min} above) are the extreme errors, and typ is the root-square-sum of the typical errors due to each rate.

[b]The T_k bias produced by a 75% decrease in k_{CO2-O}, as suggested by laboratory measurements, is 0.7, 1.9, 6, and 16 K at 80, 84, 92, and 100 km, respectively (see text).

[c]Rates are given in 10^{-11}cm^{3}s^{-1}.

Table 3. Uncertainties in Retrieved Kinetic Temperature due to the Specified Uncertainty in the Collisional Rate for Polar Winter Conditions[a]

z (km)	$k_{CO2\text{-}air}$			$k_{CO2\text{-}O}$[b]			k_{vv}			Total		
	−25%	25%	typ	−50%	50%	typ	1.2[c]	2.4[c]	typ	max[−]	max[+]	typ
104	0.0	0.0	±0.0	10	−3.2	±7.4	−0.1	−1.0	±0.7	−3.2	11	±7.4
100	−0.1	0.0	±0.1	6.1	−2.3	±4.6	−0.2	−1.0	±0.8	−2.7	6.7	±4.7
96	−0.1	0.0	±0.0	2.8	−0.9	±2.1	−0.8	−1.1	±0.9	−1.9	2.8	±2.3
92	−0.1	0.1	±0.1	0.5	0.0	±0.4	−0.2	−0.4	±0.4	−0.3	0.5	±0.5
88	0.0	0.1	±0.1	−0.2	0.3	±0.2	−0.4	−0.2	±0.3	−0.7	0.5	±0.4
84	−0.1	−0.1	±0.1	1.5	−0.8	±1.2	−0.5	−0.1	±0.4	−0.8	1.8	±1.2
80	0.5	−0.4	±0.4	0.7	−0.4	±0.6	0.1	−0.2	±0.2	−0.9	1.3	±0.8
76	0.4	−0.3	±0.4	0.1	−0.1	±0.1	0.4	−0.4	±0.4	−0.7	0.9	±0.5

[a]Temperatures are given in K. The set of rate constant values producing the maximum errors max[−] and max[+] are as in midlatitudes (see Table 2).
[b]The T_k bias produced by a 75% decrease in $k_{CO2\text{-}O}$, as suggested by laboratory measurements, is 1.3, 3, 1.5, and 14 K at 80, 84, 92, and 100 km, respectively (see text).
[c]Rates are given in $10^{-11} cm^3 s^{-1}$.

rate coefficient around 90 km and also below 80 km (the latter because atomic oxygen abundance rapidly decreases).

[32] The average global SABER T_k errors due to process 2 uncertainty are similar to those reported for other experiments, for example, CRISTA [*Gusev et al.*, 2006], being slightly smaller below 90 km and larger above.

[33] In this work, we have assumed a $k_{CO2\text{-}O}$ of $6 \times 10^{-12} cm^3 s^{-1}$ at 300 K with an uncertainty of [−50%, +50%]. All determinations of this rate constant from atmospheric measurements lie within that range. However, laboratory measurements point to a value around half of the lower limit considered here. Even if the aeronomic evidence does not support that low value (see above), we have also calculated the change in the kinetic temperature that would result when lowering the nominal rate constant by a factor of 4. The differences in T_k are then 2−3 times larger than those obtained when dividing $k_{CO2\text{-}O}$ by 2 (see footnote b in Tables 2, 3, and 4).

[34] Although, the atomic oxygen number density is not a non-LTE parameter, the sensitivity of T_k to its uncertainty is similar to that of the uncertainty in the CO_2-O quenching rate. As mentioned in the previous section, v1.07 T_k retrieval assumes daytime O vmr below about 95 km derived using SABER O_3 retrieval of 1.27 μm measurements and the $O_2(^1\Delta)$ model of *Mlynczak et al.* [1993, 2007] and NRL-MSISE-00 atomic oxygen vmr everywhere else. MSIS atomic oxygen vmr is modeled from measurements of the total oxygen amount ([O] +2[O_2]) in the

atmosphere [*Picone et al.*, 2002]. Picone et al.'s comparison of NRL-MSISE-00 molecular oxygen with that of MSIS-90 shows differences of ∼5%, which translate to a ∼10% difference in atomic oxygen between the two versions. *Gumbel* [1997] comparisons of MSIS-90 atomic oxygen with rocket-borne measurements for several seasons and latitudes show a ∼40% difference below 95 km for nighttime and ±30−40% above. More recently, *Mlynczak et al.* [2004] radiance simulations at 63 μm using MSIS atomic oxygen agreed within 10% with FIRS-2 measurements. Taking all those considerations together, we can assume an uncertainty in the atomic oxygen abundance used in SABER T_k retrieval of ±50%. The magnitude of those errors is thus similar to that produced by the $k_{CO2\text{-}O}$ rate. This error is additional to those due to the kinetic parameters.

3.3. Process 4: $CO_2^i(v_2) + CO_2^j(v_2') \rightleftharpoons CO_2^i(v_2 − 1) + CO_2^j(v_2' + 1)$

[35] The set of v_2 vibrational energy exchanges between CO_2 molecules (process 4) is important for the redistribution of the v_2 quanta among CO_2 molecules. The most important V-V process considered in this set is the exchange among CO_2 isotopes ($v_2 = 1$ and $v_2' = 0$, and $i \neq j$ in process 4 of Table 1 i.e., $CO_2^i(01^10) + CO_2^j(00^00) \rightleftharpoons CO_2^i(00^00) + CO_2^j(01^10)$), in particular, when one of the colliders is the main isotope. It also includes the most likely V-V exchange involving the higher excited levels $v_2 = 2$ and $v_2 = 3$, i.e., that with the lowest energy level of the same isotope ($v_2' = 0$

Table 4. Uncertainties in Retrieved Kinetic Temperature due to the Specified Uncertainty in the Collisional Rate for Polar Summer Conditions[a]

z (km)	$k_{CO2\text{-}air}$			$k_{CO2\text{-}O}$[b]			k_{vv}			Total		
	−25%	25%	typ	−50%	50%	typ	1.2[c]	2.4[c]	typ	max[−]	max[+]	typ
104	1.8	−0.9	±1.4	43	−16	±32	4.6	−2.2	±3.6	−18	55	±33
100	0.9	−0.5	±0.7	23	−9.8	±18	2.5	−1.3	±2.0	−11	25	±18
96	0.9	−0.5	±0.8	14	−6.3	±11	2.7	−1.3	±2.1	−7.6	15	±11
92	0.8	−0.5	±0.7	6.6	−2.6	±5.0	2.7	−1.3	±2.1	−4.0	8.1	±5.5
88	−0.4	0.1	±0.3	1.0	0.3	±0.7	0.6	0.2	±0.5	−0.1	0.7	±0.9
84	−2.3	1.6	±2.0	−2.5	1.5	±2.1	−7.1	3.4	±5.6	−8.5	6.0	±6.2
80	−1.1	0.6	±0.9	−0.3	−0.1	±0.2	−4.1	1.2	±3.0	−5.5	1.8	±3.2
76	−0.2	0.0	±0.1	−0.1	−0.2	±0.1	−0.7	0.3	±0.6	−1.5	0.4	±0.6

[a]Temperatures are given in K. We used the minimum values of the rate constants below 88 km and the maximum values above to estimate max[−], and vice versa to estimate max[+].
[b]The T_k bias produced by a 75% decrease in $k_{CO2\text{-}O}$, as suggested by laboratory measurements, is 0.1, −5, 14, and 51 K at 80, 84, 92, and 100 km, respectively (see text).
[c]Rates are given in $10^{-11} cm^3 s^{-1}$.

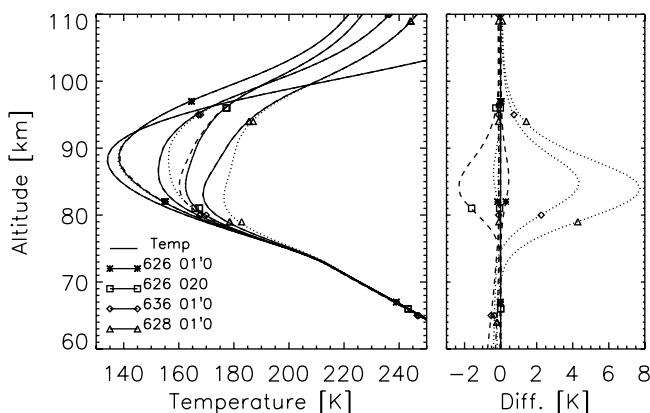**Figure 12.** Effect of the v_2-quanta V-V exchange on the $CO_2(v_2)$ vibrational temperatures (solid line denotes nominal k_{vv}, dotted line denotes $k_{vv} = 1.2 \times 10^{-11}$ cm^{3}s^{-1}, and dashed line denotes $k_{vv} = 2.4 \times 10^{-11}$ cm^{3}s^{-1}) for typical polar summer conditions. Kinetic temperature is also shown.

and $i = j$ i.e., $CO_2^i(v_2 = 2, 3) + CO_2^j(00^00) \rightleftharpoons CO_2^i(v_2 = 1) + CO_2^j(01^10))$. In this second subset of processes, the most important are the V-V exchanges within the main isotope. Process 4 mainly affects the populations of the 01^10 levels of the less abundant isotopes and, to a lesser extent, that of the 020-group (composed of the coupled triad 10^00, 02^20, 02^00; see Figure 1) and higher levels of the main isotope from 75 to 90 km. Above that altitude, quenching by atomic oxygen dominates.

[36] In an early experiment, *Rhodes et al.* [1968] indicated a rate of relaxation of the 10^00 level in V-V CO_2 exchange of 1.15×10^{-11} cm^{3}s^{-1}, although they pointed out that they could not distinguish if the 02^20 level was involved. Later interpretations of that experiment [*Seeber*, 1971] proposed that the rate measured by Rhodes et al. was more likely not related to our process 4. Additionally, Seeber calculated a rate for the 02^20 state relaxation leading to a combined relaxation rate of the 020 states of 1.6×10^{-11} cm^{3}s^{-1}.

[37] More recently, the rate at which the 020 triad levels relax to the 01^10 level through V-V exchange was measured by *Huddleston and Weitz* [1981], who reported an overall effective rate of 1.2×10^{-11} cm^{3}s^{-1}. *Dang et al.* [1983] measured, instead, the rate for the relaxation of the individual 020 levels at 280 K, concluding that the relaxation of the 02^20 level (4.7×10^{-11} cm^{3}s^{-1}) is about 20 times faster than those of the other two levels of the triad (10^00 and 02^00). Assuming the levels in the triad are in LTE among themselves (which is a good assumption since their collisions with N$_2$ and O$_2$ which couple these levels are about 2 orders of magnitude more frequent than the V-V exchange), the rates of Dang et al. yield an effective rate for the relaxation of the 020 triad of 2.4×10^{-11} cm^{3}s^{-1}, i.e., twice the value measured by Huddleston and Weitz. On the basis of theoretical arguments, *Orr and Smith* [1987] agreed with the laboratory measurements of Dang et al.

[38] Considering the harmonic oscillator law, the rate for the V-V exchange of the CO_2 isotopes in the fundamental $v_2 = 1$ state can be approximated by half of the 02^20-01^10 relaxation rate (i.e., 2.35×10^{-11} cm^{3}s^{-1} according to the

measurements of *Dang et al.* [1983]). Therefore, the rate at which the first excited level 01^10 relaxes in V-V collisions is almost equal to that at which a molecule in the 020 triad relaxes.

[39] *Kutepov et al.* [2006] showed that kinetic temperature measurements of falling spheres are consistent with SABER v1.07 T$_k$, retrieved setting the v_2 exchange rate among the CO_2 isotopes (process 4 with $v_2 = 1$ and $v_2' = 0$) to 2.4×10^{-11} cm^{3}s^{-1} and the rate constant for the effective relaxation of the 020 triad to 1.2×10^{-11} cm^{3}s^{-1}, i.e., two times smaller than for the interisotope exchange. Those are the nominal rate constants used here. This combination represents an intermediate case between that provided by *Dang et al.* and that by *Huddleston and Weitz* [1981]; actually slightly closer to that of *Dang et al.* [1983] since the interisotope $v_2 = 1$ exchange has a greater effect. We have estimated the errors assuming the same rate constant for both the isotope relaxation and the 020 triad relaxation in V-V v_2 collisions (denoted by k_{vv}), setting it to 1.2×10^{-11} cm^{3}s^{-1} (based on work by Huddleston and Weitz) and 2.4×10^{-11} cm^{3}s^{-1} (based on work by Dang et al.).

[40] The CO_2 V-V v_2 exchange mainly affects the population of the minor isotope v_2 states and, to a lesser extent, the 020 and higher v_2 levels of the main isotope in the upper mesosphere. Those levels are significantly more affected than the 01^10 state of the main isotope because the latter contains the majority (94%) of the v_2 excited molecules and, thus, this process produces only a small relative change of its population. The interisotope V-V exchange acts to depopulate the minor isotope states in favor of the 01^10 state of the main isotope. In case of V-V exchange within the same isotope, this process depopulates the higher energy level involved.

[41] The effect is largest under polar summer conditions because the levels are then farther away from LTE. Therefore, as pointed out by *Kutepov et al.* [2006], it is important to include this process in the retrieval to obtain an accurate kinetic temperature in the polar summer mesopause. In Figure 12, we show the effect of changing k_{vv} on the vibrational temperatures for a typical polar summer temperature profile. When considering the smallest k_{vv} rate constant for all v_2 exchange processes (i.e., reducing only the interisotope V-V exchange rate by a factor of 2 but keeping the nominal rate for V-V exchange within the same isotope; see discussion above), only the vibrational temperatures of the 01^10 levels of the weakest isotopes are significantly affected. The populations of these levels, mainly driven by absorption of radiation from the warmer region below, tend then to increase at altitudes from 75 to 90 km (where their contribution to SABER 15 μm radiance is important) since they become less coupled to the main isotope 01^10 state, which has a lower vibrational temperature. The T$_v$ decrease in the example shown is 4 K for 636-01^10 and up to 8 K for 628-01^10. Therefore, the retrieved T$_k$ for a slower k_{vv} rate is smaller than the nominal temperature at those altitudes.

[42] The errors in the kinetic temperature for the equinox and the solstice days considered here (18 March and 15 July 2004) are shown in Figure 13 (top). They do not exceed 0.5 K at any altitude, latitude or season except close to the polar summer, where the T$_k$ error around 84 km ranges from -2 K at 40°N to -7 K at 82°N (during 15 July 2004). Although this process barely affects the vibrational level population above 90 km (see Figure 12), the temperature
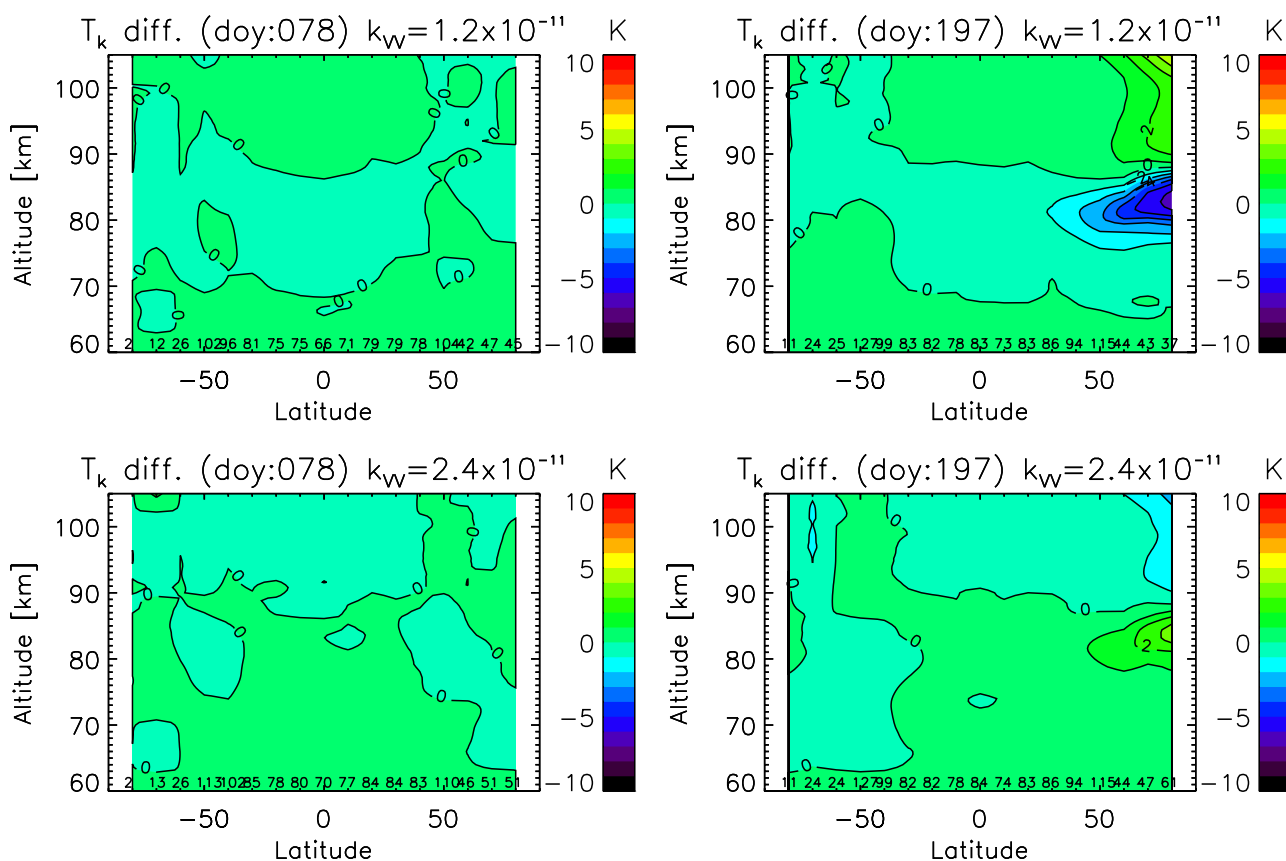
Figure 13. As in Figure 8 but for the uncertainty in CO_2 V-V ν_2-quanta exchange rate for (top) $k_{vv} = 1.2 \times 10^{-11}$ cm^3s^{-1} and (bottom) $k_{vv} = 2.4 \times 10^{-11}$ cm^3s^{-1}. Contours are plotted every 1 K.

slightly increases above 90 km around the polar summer (by ~2 K) for a slower rate. The temperature decrease around the mesopause resulting from the decrease in the k_{vv} rate constant causes a decrease in pressure which, through hydrostatics, extends to higher altitudes. This decrease in pressure above 90 km is then compensated by a small increase in temperature in order to restore the total density (and thus CO_2 density) to match the measured radiance.

[43] When considering the largest k_{vv} rate constant (2.4×10^{-11} cm^3 s^{-1}) for all ν_2 exchange processes (i.e., doubling the k_{vv} involving the $\nu_2 \geq 2$ states and keeping the nominal k_{vv} for the interisotope exchange; see discussion above), only the population of the 020-group and upper levels are significantly affected (see Figure 12). The vibrational temperature of the 020 levels tends to decrease (2 K at 85 km in polar summer conditions). The effect on the retrieved T_k is negligible under most atmospheric conditions except at latitudes close to the summer pole (see Figure 13, bottom), where T_k increases at 80–90 km causing the largest error of 3 K at 84 km. The effect of doubling the rate of the process involving the 020 and higher states is smaller than halving the interisotope V-V $\nu_2 = 1$ exchange rate because the latter is a more important process.

3.4. Overall Errors

[44] Tables 2, 3, and 4 summarize the errors on SABER T_k due to the uncertainty (as indicated in each column) of each non-LTE kinetic parameter for midlatitudes, polar summer and polar winter, respectively. The midlatitude

errors are an average of the errors estimated for T_k profiles measured at latitudes within [35°N, 55°N] and [35°S, 55°S] during equinox and solstice (18 March and 15 July 2004). The errors for polar conditions are the average of the errors of profiles within 10° around the corresponding polar latitude in the solstice case. For each rate constant, the column labeled with "typ" shows the typical error, estimated with the quadratic average of the errors in both directions.

[45] We also report in Tables 2, 3, and 4 the extreme errors (max^- and max^+) obtained by setting the rate constants of the four processes 1−4 within their uncertainty range to produce the largest deviations (in both senses) from the nominal case. Those errors represent the less favorable and rather conservative cases because all rate constants used then act on the nominal T_k in the same direction. The set of constants used for each case to obtain max^- and max^+ are also indicated in Tables 2, 3, and 4. In midlatitudes and polar winter, the maximum deviation from the nominal temperature profile max^- is produced for the maximum $k_{CO2\text{-}air}$ and $k_{CO2\text{-}O}$ values (within the uncertainty ranges provided here), and the minimum k_{vv} value below 88 km and its maximum value above that altitude. The maximum deviation in the opposite sense (max^+) is obtained by setting $k_{CO2\text{-}air}$ and $k_{CO2\text{-}O}$ to their minimum values, and k_{vv} to its maximum value below 88 km and its minimum value above. For polar summer, the maximum deviation from the nominal kinetic temperature (max^-) is obtained with minimum $k_{CO2\text{-}air}$, $k_{CO2\text{-}O}$ and k_{vv} values below 88 km and
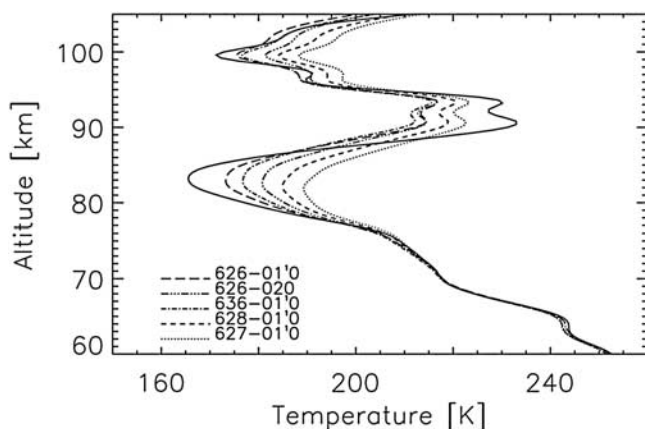
Figure 14. CO_2 vibrational temperatures for the main emitting levels at 15 μm for a scan taken on 15 January 2003.

maximum values above, and vice versa for the maximum deviation in the opposite sense (max$^+$).

[46] The combined error of all rates, i.e., the root-sum-square of the typical errors due to each parameter uncertainty, which represent the (typical size) estimated total errors in SABER v1.07 kinetic temperature due to uncertainties in the non-LTE parameters is also listed in Tables 2, 3, and 4. The largest typical total errors correspond to polar summer, where the most significant occur around the mesopause ($\pm$6 K) and above 92 km (>6 K, in absolute value). At midlatitudes, the typical errors are smaller (in absolute value) than $\pm$1.5 K below 96 km and smaller than $\pm$8 K below 104 km. In polar winter, the errors are slightly larger than at midlatitudes above 96 km, where they reach $\pm$5 K and $\pm$7 K at 100 km and 104 km, respectively.

[47] It is worth noting that the change of the T_k errors with the solar zenith angle (SZA) is small. On the one hand, even if the CO_2 upper levels are indirectly pumped by solar radiation, the 626-01^{1}0 level (main responsible for SABER 15 μm radiance; see Figure 2) is barely affected by the SZA [*López-Puertas and Taylor*, 2001]. On the other hand, the variation of atomic oxygen with SZA is largest below 85–90 km, where the effect of the rate uncertainties is small (except for polar summer around 85 km). As a consequence, the dependence of the errors on SZA is a second-order effect as compared with the dependence on the temperature structure, i.e., latitude or strong inversion layers. The differences in the overall error between maximum and minimum SZAs for a similar temperature profile are smaller than 0.5 K and 1 K for midlatitudes and polar summer, respectively.

3.5. Errors in Tide and Inversion Layer Temperature Amplitudes and in Other Particular Cases

[48] In the previous sections we have addressed the effect of the kinetic parameters on the retrieved kinetic temperature for scenarios with smooth temperature profiles. However, these effects strongly depend on the actual vertical temperature structure and, hence, on the presence or absence of inversion layers. This applies in particular to the regions where the tides are stronger, i.e., at low latitudes, or when some other heating or cooling mechanisms produce oscillating signatures in the temperature profile.

[49] A typical example for these conditions is that of Figure 14, where we show the SABER kinetic temperature together with the vibrational temperatures for the main CO_2 v_2 levels for an individual profile close to the equator. The kinetic temperature abruptly increases around 85 km by 70 K in only 5 km. Under these conditions, the quenching of $CO_2(v_2)$ by other molecules is not fast enough to bring their populations to LTE, resulting in a large departure from LTE and, hence, the vibrational level populations are more sensitive to the uncertainties in the non-LTE collisional rates. The maximum errors in T_k are found at the altitude of crests and troughs of the inversion layer. Their magnitude depends not only on the inversion layer amplitude but also on its altitude. For this individual example, the maximum errors in the kinetic temperature caused by the uncertainty in the quenching rate of $CO_2(v_2)$ by N_2 and O_2 ($k_{CO2\text{-air}}$), by O ($k_{CO2\text{-O}}$), and the V-V v_2-quanta exchange rate (k_{vv}) are, respectively, $\pm$1.4 K (at 82 km), $\pm$8 K (at 90 km) and $\pm$2.8 K (at 82 km) (see Figure 15). The overall errors in the crests and troughs of this particular profile are $\pm$3.5 K at 82 km, $\pm$8 K at 90 km and $\pm$1.6 at 100 km.

[50] These enhanced T_k errors around the inversion layers might affect the tidal analysis based on SABER temperatures. We have estimated the errors affecting diurnal tide amplitudes from the differences between the mean temperature of the ascending segment scans of an orbit minus that of the descending one at equatorial latitudes. We performed these calculations for SABER measurements taken during the north viewing phase of 15 July 2004. The average temperatures for the ascending and descending portions are shown in Figure 16 (left). For this particular period, the equatorial local time (LT) for the ascending scans was 2300 LT. whereas that for the descending ones was 1400 LT, i.e., about 9 hours apart. Figure 16 also shows the ascending minus the descending mean temperatures divided by two (referred hereafter as amplitude) together with the overall effect of the $k_{CO2\text{-air}}$, $k_{CO2\text{-O}}$ and k_{vv} rate uncertainties (Figure 16, middle). The oscillating structure of the difference, with a vertical wavelength of about 20 km, and with increasing amplitude in the mesosphere is typical of a diurnal tide signature. The error in the amplitude is shown in Figure 16 (right). The errors in the amplitude are negligible below 80 km. For the amplitude of ~16 K at 88 km of our example, the overall error is $\pm$1.5 K, mostly due to the uncertainty in the V-V v_2 exchange rate and to a much lesser extent to the rate of CO_2 quenching by N_2 and O_2. The amplitude at 95 km has an error of $\pm$3 K, which is almost totally due to the uncertainty in the CO_2-O quenching. The errors in the phase are negligible.

[51] An additional source of error in the estimation of the tidal amplitude might come from an inaccurate inclusion of the tide effect on the atomic oxygen used in the T_k retrieval. In principle, the effect through the total density (with which the O density is calculated from the O vmr profiles) is taken into account because SABER measures pressure and temperature. Additionally, the O vmr profiles also include, to a first order, the tidal effects since, for daytime cases below 95 km, it is simultaneously measured by SABER and, for any other case, it comes from NRL-MSIS-00, which also incorporates tides [*Picone et al.*, 2002]. Nevertheless, we have checked how well the tide shows up in the O vmr for our example in Figure 16. If chemical effects on O are
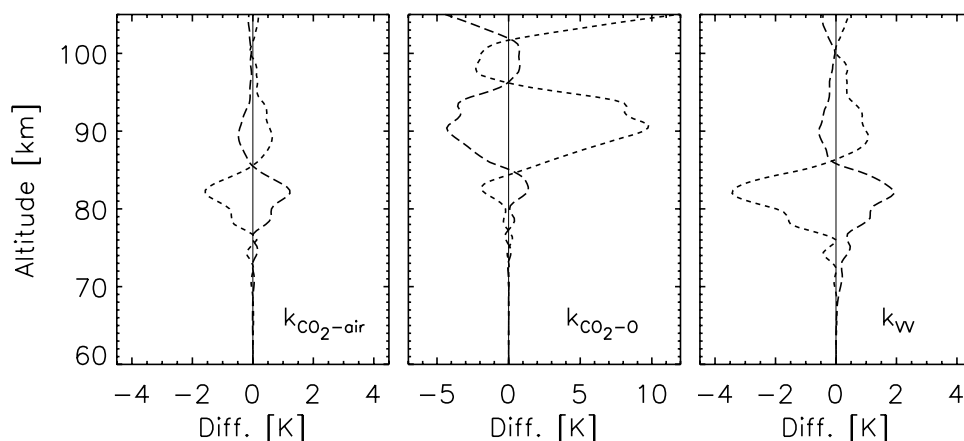
Figure 15. Error in the kinetic temperature of the scan in Figure 14 due to minimum (short-dashed line) and maximum (long-dashed line) values assumed for the quenching rate of $CO_2(v_2)$ by (left) N_2 and O_2, (middle) O, and (right) the V-V v_2-quanta exchange rate. Note the different scales of the x axes.

negligible (valid assumption above 85–90 km [*Smith et al.*, 2003]), the O vmr deviation from the daily average produced by a tide can be estimated from the T_k deviation, once the O vertical gradient and the static stability are known [see *Smith et al.*, 2003, expression (5)]. Accordingly, the tide of our example, which causes variations of ±16 K at 88 km and 95 km, should produce a O vmr variation (in phase with the T_k variation) of ±50–70% and ±30–40%, respectively. The deviations of both the ascending and the descending average O vmr profiles used in the retrieval with respect to the daily average are 110% at 88 km and 40% and 95 km, also in phase with the T_k variation (not shown). Hence, the effect of the tide on the atomic oxygen is correctly represented at 95 km but it is overestimated at 88 km by 50% (although within the estimated O uncertainty; see section 3.2). That means that the O vmr at 88 km is underestimated by 50% for the descending average and overestimated by 50% for the ascending average, which translates into an underestimation of T_k of 1 K and 4 K, respectively; that is, both act in the same sense. Consequently, the impact on the amplitude of inaccuracies in the inclusion of O vmr tidal effects is an underestimation of 1.5 K at 88 km but no error at 95 km.

[52] There are other particular scenarios where the thermal structure differs strongly from the typical cases studied in previous sections. That is the case for the anomalous high stratopause measured by SABER at high northern latitudes during January and February of 2004 and 2006. This feature was attributed by *Siskind et al.* [2007] to a highly disturbed lowermost stratosphere which blocked the gravity waves impeding the warming around the usual stratopause altitudes. The T_k errors due to non-LTE rate constants under these conditions behave similarly to those around the inversion layers. However, these errors can extend downward depending on the stratopause altitude (as they did with the inversion layer altitude). Figure 17 shows the zonal mean kinetic temperature at 80°N for January 15th 2004, together with the vibrational temperatures for the main CO_2 v_2 levels. The altitude of the 260-K stratopause was located at 80 km. The CO_2 v_2 state populations depart strongly from LTE and they do so from uncommonly low altitudes (from 60 km for the nominal case). The effect of the uncertainty in

the k_{vv} rate on the kinetic temperature (not shown) starts being important at altitudes as low as 60 km, and increases from ±1.3 K at 64 km to its maximum of ±2 K at 75 km in this case. It is negligible above 80–85 km. The effect of the CO_2-O quenching rate uncertainty is noticeable above 75 km, reaching its maximum of ±5 K at 84 km. The effect of the $k_{CO2\text{-air}}$ rate uncertainty is always smaller than ±1 K. Thus, the errors under these circumstances become important at lower altitudes and are larger than for typical T_k profiles.

[53] In the extreme cases presented in this section, the error in the SABER T_k might further affect other atmospheric quantity retrievals that need accurate knowledge of the temperature profile. That is the case of mesospheric ozone and water vapor retrieved from SABER 9.6 and 6.3 μm radiance, respectively. The impact of the T_k errors in the MLT region on other SABER products is outside the scope of this paper and will be subject of a future analysis.
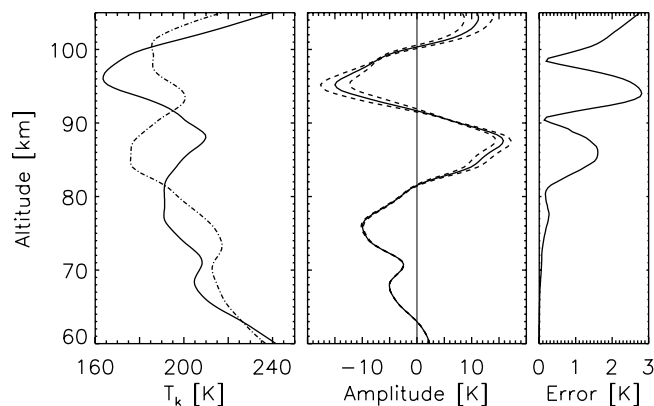

Figure 16. (left) Average temperature for the ascending (solid line) and descending (dash-dotted line) SABER scans around the equator during the north viewing phase for 15 July 2004. (middle) Difference (ascending-descending) divided by 2 for the nominal case (solid line), the minimum (short-dashed line) and the maximum (long-dashed line) values of the collisional rates. (right) Overall error in the difference divided by 2.
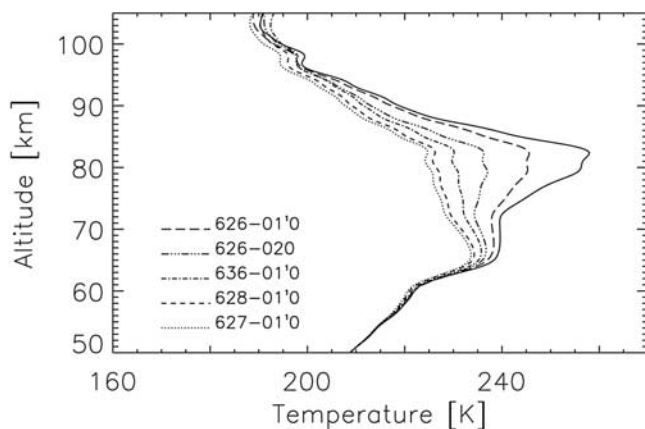
Figure 17. SABER kinetic temperature (solid line) and $CO_2(v_2)$ vibrational temperatures (labels are as described in Figure 5) averaged for measurements taken around 80°N during 15 January 2004. The anomalously high stratopause provokes the CO_2 levels to depart from LTE at unusual low altitudes.

However, it is important to note that, even considering the enhanced errors found under these extreme conditions, the non-LTE SABER T_k retrievals in the MLT are more accurate precisely owing to the use of non-LTE algorithms.

4. Summary and Conclusions

[54] At the time of this publication, the SABER instrument has provided global middle atmosphere kinetic temperature derived from 15 μm limb radiance measurements for more than 6 years. Non-LTE algorithms are used to retrieve the temperature in the mesosphere and lower thermosphere from SABER measurements [*Mertens et al.*, 2001]. The SABER v1.07 kinetic temperature is validated by *Remsberg et al.* [2008], who, together with the error estimates due to non-LTE parameters presented in this work, provide an estimate of the systematic error due to CO_2 abundance uncertainty (1.3 K at 80 km, 3.6 K at 90 km and 1.4 K at 100 km) and of the noise error (1.8 K at 80 km, 3.6 K at 90 km and 6.7 K at 100 km for midlatitudes, and 2.7 K at 80 km, 8.9 K at 90 km and 8.9 K at 100 km for polar summer). In this paper, we have evaluated the systematic errors in the SABER operationally retrieved kinetic temperature (version 1.07) due to the current uncertainties in the collisional rates of the non-LTE model for the typical midlatitude conditions and also for extreme conditions. The summary of our findings follows.

[55] 1. The response of the operational SABER T_k retrieval scheme to perturbations of the collisional rates behaves as expected from non-LTE theory. This is confirmed by the fact that increasing the rates produces the opposite response to that when decreasing the rates at all altitudes, latitudes and seasons. The systematic error estimations performed in this work for typical and extreme atmospheric conditions can, in consequence, be interpolated to other intermediate atmospheric conditions.

[56] 2. The overall error in the retrieved kinetic temperature is around $\pm 1-2$ K below 95 km for midlatitudes and polar winter, and below 80 km for polar summer. The error is around ± 4 K at 100 km in midlatitudes and ± 5 K in polar

winter. In polar summer, the error is significantly larger, ± 6 K at 85 km, but decreases to ± 1 K at 88 km and increases to ± 18 K at 100 km.

[57] 3. Under most conditions, the overall T_k error due to the non-LTE kinetic parameters is mainly due to the uncertainty in the quenching rate of $CO_2(v_2)$ by atomic oxygen. Under polar summer conditions, the uncertainty in the rate of V-V v_2-quanta exchange also contributes significantly to the overall temperature error below 90 km.

[58] 4. Below 74 km the retrieved T_k errors are smaller than 0.5 K in both the typical and the extreme atmospheric scenarios considered.

[59] 5. Temperatures retrieved in polar summer scenarios have the largest errors because the CO_2 vibrational levels populations are farther away from LTE conditions and therefore they are more sensitive to the uncertainties in the collisional rates.

[60] 6. Except for situations in which a vertical temperature structure in the mesosphere and lower thermosphere is significant, the errors in equinox conditions are latitude-independent and similar to those at midlatitudes.

[61] 7. The errors are somewhat larger when the temperature profiles have pronounced vertical structure, even outside the polar summer. The overall errors in those cases can rise up to ± 3 K around 80 km and ± 8 K at 90 km if crests or troughs are present at those altitudes. This affects the estimate of wave temperature amplitudes from SABER data, which can be affected by errors due to non-LTE kinetic parameter uncertainties of ± 3 K.

[62] In order to reduce these systematic errors and raise the altitude at which the SABER T_k is accurately derived, it is essential to know with a better accuracy the CO_2-O quenching rate and, in particular, to understand why the measurements in the laboratory differ by a factor of 4 with respect to the ones derived from atmospheric observations. It is also necessary to determine the CO_2 v_2 vibrational energy transfer rate with a higher accuracy since the published measurements, which date from the eighties, differ by a factor of 2.

[63] In spite of the error analysis presented here, the kinetic temperature measured by SABER provides an unprecedented opportunity to achieve a deep understanding of the physics of the mesosphere and lower thermosphere as, for the first time, it is operationally derived in that atmospheric region from continuous space flight instrument measurements. Additionally, the SABER experiment is providing temperature retrievals that are more nearly correct for all of the extreme situations presented in this work thanks to its non-LTE algorithm.

References

Allen, D. C., T. J. Price, and J. S. M. C.Simpson (1977), Vibrational deactivation of the bending mode of CO_2 measured between 1500 K and 150 K, *Chem. Phys. Lett.*, *45*, 183–187.

Allen, D. C., T. Scragg, and J. S. M. C.Simpson (1980), Low temperature fluorescence studies of the deactivation of the bend-stretch manifold of CO_2, Chem. Phys., 51, 279–298.

Castle, K. J., K. M. Kleissas, J. M. Rhinehart, E. S. Hwang, and J. A. Dodd (2006), Vibrational relaxation of CO_2 (v_2) by atomic oxygen, J. Geophys. Res., 111, A09303, doi:10.1029/2006JA011736.

Dang, C., J. Reid, and B. K. Garside (1983), Dynamics of the CO_2 upper laser level as measured with a tunable diode laser, Appl. Phys. B, 31, 163–172.

Fleming, E. L., S. Chandra, J. J. Barnett, and M. Corney (1990), Zonal mean temperature, pressure, zonal winds and geopotential heights as function of latitude, Adv. Space Res., 10, 1211–1259.

García, R. R., D. R. Marsh, D. E. Kinnison, B. A. Boville, and F. Sassi (2007), Simulations of secular trends in the middle atmosphere, 1950–2003, J. Geophys. Res., 112, D09301, doi:10.1029/2006JD007485.

Gille, J. C., and F. B. House (1971), On the inversion of limb radiance measurements. I: Temperature and thickness, J. Atmos. Sci., 28, 1427–1442.

Grossmann, K. U., D. Offermann, O. Gusev, J. Oberheide, M. Riese, and R. Spang (2002), The CRISTA-2 mission, J. Geophys. Res., 107(D23), 8173, doi:10.1029/2001JD000667.

Gumbel, J. (1997), Rocket-borne optical measurements of minor constituents in the middle atmosphere, Ph.D. thesis, Stockholm Univ., Stockholm.

Gusev, O., M. Kaufmann, K. U. Grossmann, F. J. Schmidlin, and M. G. Shepherd (2006), Atmospheric neutral temperature distribution at the mesopause/turbopause altitude, J. Atmos. Sol. Terr. Phys., 68(15), 1684, doi:10.1016/j.jastp.2005.12.010.

Huddleston, R. K., and E. Weitz (1981), A laser-induced fluorescence study of energy transfer between the symmetric stretching and bending modes of CO_2, Chem. Phys. Lett., 83, 174–179.

Khvorostovskaya, L. E., I. Y. Potekhin, G. M. Shved, V. P. Ogibalov, and T. V. Usyukova (2002), Measurement of rate constant for quenching CO_2 [01^10] by atomic oxygen at low temperatures: Reassessment of the rate of cooling by the CO_2 15-μm emission in the lower thermosphere, Izv. Atmos. Oceanic Phys., 38, 613–624.

Kutepov, A. A., A. G. Feofilov, B. T. Marshall, L. L. Gordley, W. D. Pesnell, R. A. Goldberg, and J. M. Russell III (2006), SABER temperature observations in the summer polar mesosphere and lower thermosphere: Importance of accounting for the CO_2 v_2 quanta V–V exchange, Geophys. Res. Lett., 33, L21809, doi:10.1029/2006GL026591.

Lilenfeld, H. V. (1994), Deactivation of vibrationally-excited NO and CO_2 by O-atoms, Tech. Rep. PL-TR-94-2180, 28 pp., Air Force Phillips Lab., Bedford, Mass.

López-Puertas, M., and F. W. Taylor (2001), Non-LTE Radiative Transfer in the Atmosphere, World Sci., Tokyo.

López-Puertas, M., R. Rodrigo, A. Molina, and F. W. Taylor (1986), A non-LTE radiative transfer model for infrared bands in the middle atmosphere. I. Theoretical basis and application to CO_2 15 μm bands, J. Atmos. Terr. Phys., 48, 8499–8513.

López-Puertas, M., M. A. López-Valverde, C. P. Rinsland, and M. R. Gunson (1992), Analysis of the upper atmosphere CO_2 (v_2) vibrational temperatures retrieved from ATMOS/Spacelab 3 observations, J. Geophys. Res., 97, 20,469–20,478.

López-Puertas, M., G. Zaragoza, M. A. López-Valverde, and F. W. Taylor (1998), Nonlocal thermodynamic (LTE) atmospheric limb emission at 4.6 μm: 1. An update of the CO_2 non-LTE radiation transfer model, J. Geophys. Res., 103, 8499–8513.

Lunt, S. L., C. T. Wickham-Jones, and J. S. M. C.Simpson (1985), Rate constants for the deactivation of the 15μm band of carbon dioxide by the collisions partners Ch_3F, CO_2, N_2, Ar and Kr over the temperature range 300 to 150 K, Chem. Phys. Lett., 115, 60–64.

Marshall, B. T., L. L. Gordley, and D. A. Chu (1994), BANDPAK: Algorithms for modeling broadband transmission and radiance, J. Quant. Spectrosc. Radiat. Transfer, 52, 581–599.

Mertens, C. J., M. G. Mlynczak, M. López-Puertas, P. P. Wintersteiner, R. H. Picard, J. R. Winick, L. L. Gordley, and J. M. Russell III (2001), Retrieval of mesospheric and lower thermospheric kinetic temperature from measurements of CO_2 15 μm Earth limb emission under non-LTE conditions, Geophys. Res. Lett., 28, 1391–1394.

Mertens, C. J., M. G. Mlynczak, M. López-Puertas, P. P. Wintersteiner, R. H. Picard, J. R. Winick, L. L. Gordley, and J. M. Russell III (2002), Retrieval of kinetic temperature and carbon dioxide abundance from nonlocal thermodynamic equilibrium limb emission measurements made by the SABER experiment on the TIMED satellite, Proc. SPIE Int. Soc. Opt. Eng., 4882, 162–171.

Mlynczak, M. G., S. Solomon, and D. S. Zaras (1993), An updated model for O_2 ($a^1\Delta g$) concentrations in the mesosphere and lower thermosphere and implications for remote sensing of ozone at 1.27 μm, J. Geophys. Res., 98, 18,639–18,648.

Mlynczak, M. G., F. J. Martin-Torres, D. G. Johnson, D. P. Kratz, W. A. Traub, and K. Jucks (2004), Observations of the O (^3P) fine structure line at 63 μm in the upper mesosphere and lower thermosphere, J. Geophys. Res., 109, A12306, doi:10.1029/2004JA010595.

Mlynczak, M. G., B. T. Marshall, F. J. Martin-Torres, J. M. Russell, R. E. Thompson, E. E. Remsberg, and L. L. Gordley (2007), Sounding of the Atmosphere using Broadband Emission Radiometry observations of daytime mesospheric O_2 ($^1\Delta$) 1.27 μm emission and derivation of ozone, atomic oxygen, and solar and chemical energy deposition rates, J. Geophys. Res., 112, D15306, doi:10.1029/2006JD008355.

Orr, J. B., and I. W. M. Smith (1987), Collision-induced vibrational energy transfer in small polyatomic molecules, J. Phys. Chem., 91, 6106–6119.

Picone, J. M., A. E. Hedin, D. P. Drob, and A. C. Aikin (2002), NRLMSISE-00 empirical model of the atmosphere: Statistical comparisons and scientific issues, J. Geophys. Res., 107(A12), 1468, doi:10.1029/2002JA009430.

Pollock, D. S., G. B. I. Scott, and L. F. Phillips (1993), Rate constant for quenching CO_2 (010) by atomic oxygen, Geophys. Res. Lett., 20, 727–729.

Remsberg, E. E., et al. (2008), Assessment of the quality of the Version 1.07 temperature-versus-pressure profiles in the middle atmosphere from TIMED/SABER, J. Geophys. Res., 113, D17101, doi:10.1029/2008JD010013.

Rhodes, C. K., M. J. Kelly, and A. Javan (1968), Collisional relaxation of the 10^00 State in Pure CO_2, J. Chem. Phys., 48, 5730–5731, doi:10.1063/1.1668665.

Russell, J. M., III, M. G. Mlynczak, L. L. Gordley, J. Tansock, and R. Esplin (1999), An overview of the SABER experiment and preliminary calibration results, Proc. SPIE Int. Soc. Opt. Eng., 3756, 277–288.

Seeber, K. N. (1971), Radiative and collisional transitions between coupled vibrational modes of CO_2, J. Chem. Phys., 55, 5077–5081, doi:10.1063/1.1675625.

Sharma, R. D., and P. P. Wintersteiner (1990), Role of carbon dioxide in cooling planetary atmospheres, Geophys. Res. Lett., 17, 2201–2204.

Shved, G. M., L. E. Khvorostovskaya, I. Y. Potekhin, A. I. Dem'Ryanikov, A. A. Kutepov, and V. I. Fomichev (1991), Measurement of the quenching rate constant of CO_2 (01^10)-O collisions and its significance for the thermal regime and radiation in the lower thermosphere, Atmos. Oceanic Phys., 27, 295–299.

Siddles, R. M., G. J. Wilson, and J. S. M. C.Simpson (1994), The vibrational deactivation of the [00^01] and [01^00] modes of CO_2 measured down to 140 K, Chem. Phys., 189, 779–791.

Simpson, C. J. S. M., P. D. Gait, and J. M. Simmie (1977), The vibrational deactivation of the bending mode of CO_2 by O_2 and by N_2, Chem. Phys. Lett., 47, 133–136.

Siskind, D. E., S. D. Eckermann, L. Coy, J. P. McCormack, and C. E. Randall (2007), On recent interannual variability of the Arctic winter mesosphere: Implications for tracer descent, Geophys. Res. Lett., 34, L09806, doi:10.1029/2007GL029293.

Smith, A. K., D. R. Marsh, and A. C. Szymczak (2003), Interaction of chemical heating and the diurnal tide in the mesosphere, J. Geophys. Res., 108(D5), 4164, doi:10.1029/2002JD002664.

Taine, J., and F. Lepoutre (1979), A photoacoustic study of the collisional deactivation of the first vibrational levels of CO_2 by N_2 and CO, Chem. Phys. Lett., 65, 554–558.

Taine, J., F. Lepoutre, and G. Louis (1978), A photoacoustic study of the collisional deactivation of CO_2 by N_2, CO and O_2 between 160 and 375 K, Chem. Phys. Lett., 58, 611–615.

Vollman, K., and K. U. Grossmann (1997), Excitation of 4.3 μm CO_2 emissions by O (^1D) during twilight, Adv. Space Res., 20, 1185–1189.

Wintersteiner, P. P., R. H. Picard, R. D. Sharma, J. R. Winick, and R. A. Joseph (1992), Line-by-line radiative excitation model for the nonequilibrium atmosphere: Application to CO_2 15-microns emission, J. Geophys. Res., 97, 18,083–18,117.

————————————

D. Bermejo-Pantaleón, B. Funke, M. García-Comas, and M. López-Puertas, Instituto de Astrofísica de Andalucía, CSIC, Apartado de Correos 3004, E-18080 Granada, Spain. (diego@iaa.es; bernd@iaa.es; maya@iaa.es; puertas@iaa.es)

L. L. Gordley and B. T. Marshall, G & A Technical Software, 1864 Canon Boulevard, Suite 101, Newport News, VA 23606, USA. (l.l.gordley@gats-inc.com; b.t.marshall@gats-inc.com)

C. J. Mertens, M. G. Mlynczak, and E. E. Remsberg, NASA Langley Research Center, Hampton, VA 23681-0001, USA. (christopher.j.mertens@nasa.gov; Martin.G.Mlynczak@nasa.gov; ellis.e.remsberg@nasa.gov)

J. M. Russell III, Center for Atmospheric Sciences, Hampton University, Hampton, VA 23668, USA. (james.russell@hamptonu.edu)

P. P. Wintersteiner, ARCON Corporation, 260 Bear Hill Road, Waltham, MA 02154, USA. (winters@arcon.com)